Dual-Energy CT for Imaging of Pulmonary Hypertension: Challenges and Opportunities[1]

Seyed Ameli-Renani, MBBS, FRCR
Farzana Rahman, MBBS, FRCR
Arjun Nair, MD, MRCP, FRCR
Laurie Ramsay, BMBCh
Jenny Louise Bacon, BM, MRCP
Alex Weller, MBBS, FRCR
Heminder K. Sokhi, MBBCh, FRCR
Anand Devaraj, MD, MRCP, FRCR
Brendan Madden, MBBS, FRCP, FRCPI
Ioannis Vlahos, MRCP, FRCR

Computed tomography (CT) is routinely used in the evaluation of patients with pulmonary hypertension (PH) to assess vascular anatomy and parenchymal morphology. The introduction of dual-energy CT (DECT) enables additional qualitative and quantitative insights into pulmonary hemodynamics and the extent and variability of parenchymal enhancement. Lung perfusion assessed at pulmonary blood volume imaging correlates well with findings at scintigraphy, and pulmonary blood volume defects seen in pulmonary embolism studies infer occlusive disease with increased risk of right heart dysfunction. Similarly, perfusion inhomogeneities seen in patients with PH closely reflect mosaic lung changes and may be useful for severity assessment and prognostication. The use of DECT may increase detection of peripheral thromboembolic disease, which is of particular prognostic importance in patients with chronic thromboembolic PH with microvascular involvement. Other DECT applications for imaging of PH include low-kilovoltage images with greater inherent iodine conspicuity and iodine-selective color-coded maps of vascular perfusion (both of which can improve visualization of vascular enhancement), virtual nonenhanced imaging (which better depicts vascular calcification), and, potentially, ventricular perfusion maps (to assess myocardial ischemia). In addition, quantitative assessment of central vascular and parenchymal enhancement can be used to evaluate pulmonary hemodynamics in patients with PH. The current status and potential advantages and limitations of DECT for imaging of PH are reviewed, and current evidence is supplemented with data from a tertiary referral center for PH.

Abbreviations: CTEPH = chronic thromboembolic PH, CTPA = CT pulmonary angiography, DECT = dual-energy CT, MLA = mosaic lung attenuation, PBV = pulmonary blood volume, PH = pulmonary hypertension, PVR = pulmonary vascular resistance, RHC = right heart catheterization, V/Q = ventilation-perfusion

RadioGraphics 2014; 34:1769–1790

Published online 10.1148/rg.347130085

Content Codes: CH CT

[1]From the Department of Radiology (S.A.R., F.R., A.N., L.R., A.W., H.K.S., A.D., I.V.) and Pulmonary Hypertension Unit (J.L.B., B.M.), St George's Hospital, Blackshaw Road, London SW17 0PZ, England. Presented as an education exhibit at the 2012 RSNA Annual Meeting. Received September 24, 2013; revision requested January 22, 2014, and received February 20; accepted April 25. For this journal-based SA-CME activity, the authors J.L.B. and I.V. have provided disclosures (see p 1788); all other authors, the editor, and the reviewers have disclosed no relevant relationships. **Address correspondence to** S.A.R. (e-mail: *seyedameli@doctors.org.uk*).

See discussion on this article by Godoy (pp 1791–1792).

SA-CME LEARNING OBJECTIVES

After completing this journal-based SA-CME activity, participants will be able to:

- Discuss the role of DECT in pulmonary perfusion imaging.
- Describe the main applications of DECT to the imaging of PH.
- Identify the limitations of DECT for evaluating parenchymal perfusion and discuss possible solutions.

See www.rsna.org/education/search/RG.

TEACHING POINTS

See last page

Introduction

Pulmonary hypertension (PH) is a life-threatening condition with an insidious onset; patients frequently present late, with nonspecific symptoms that are often attributable to coexistent diseases. PH is hemodynamically defined as a mean pulmonary artery pressure of 25 mm Hg or more, with true pulmonary vascular disease characterized by a concomitant elevation in pulmonary vascular resistance (PVR) (1).

Last reclassified at the fifth World Symposium on Pulmonary Hypertension in 2013 (2), PH is categorized according to clinical groups that include idiopathic disease and disease secondary to cardiac, pulmonary, and chronic thromboembolic causes (Table). The selective availability of new treatments and the morbidity and mortality

Clinical Classification of PH

Pulmonary arterial hypertension
Idiopathic, heritable, drug- or toxin-induced, connective tissue disease–associated, human immunodeficiency virus, portal hypertension, congenital cardiac disease, pulmonary veno-occlusive disease, pulmonary capillary hemangiomatosis
PH due to left heart disease
Systolic and diastolic dysfunction and valvular disease
PH due to lung diseases and/or hypoxia
Chronic obstructive pulmonary disease, interstitial lung disease, pulmonary diseases with a mixed restrictive and obstructive pattern, sleep-disordered breathing, alveolar hypoventilation disorders, chronic high-altitude exposure
CTEPH
PH with unclear multifactorial mechanisms
Hematologic and myeloproliferative disorders, systemic disorders (eg, sarcoidosis, pulmonary Langerhans cell histiocytosis, lymphangioleiomyomatosis, neurofibromatosis, vasculitis), metabolic disorders (eg, glycogen storage disease, Gaucher disease, thyroid disorders), and other disorders (eg, tumoral obstruction, fibrosing mediastinitis, chronic renal failure on dialysis)

Note.—CTEPH = chronic thromboembolic PH.

of late diagnosis underlie the importance of early and correct diagnosis. Right heart catheterization (RHC) is the criterion standard for investigation, but it is an invasive procedure and hence not without risk. Radiologic assessment, most commonly with computed tomography (CT), is central to the evaluation of PH and can assist in elucidating the underlying cause (3,4).

In recent years, the introduction of multidetector CT systems capable of dual-energy CT (DECT) has led to a practical implementation of the imaging potential that was first proposed and investigated at the inception of CT more than 30 years ago (5). The use of dual-source systems or highly responsive detector materials that permit rapid kilovoltage switching has permitted near-simultaneous acquisitions of volumetric isotropic datasets at varying kilovoltages (6). In turn, these acquisitions permit material differentiation according to three-material decomposition mathematic algorithms. The value of DECT in thoracic imaging has been widely reported (7–9). In particular, the calculation of iodine distribution in the lung parenchyma to generate pulmonary blood volume (PBV) maps is an example of a DECT material-specific technique that augments conventional thoracic CT. This surrogate indicator of pulmonary perfusion is comparable to scintigraphy, is well established for use in evaluating acute pulmonary embolism, and correlates with disease severity and outcome (10). Increasing data and experience suggest that PBV imaging may also assist not only in the evaluation of patients with CTEPH but also in the wider evaluation of patients with PH.

In this article, we review the current use of DECT in patients with suspected or established PH, evaluate established DECT applications and evolving functions, and discuss current limitations and future potential.

Imaging Considerations in PH

RHC remains the criterion standard for identifying, quantifying, and prognosticating PH. However, RHC is an invasive procedure that requires local expertise and involves some risk and additional cost (11). Therefore, the use of an alternative, noninvasive imaging modality to reduce the need for RHC at diagnosis or follow-up is an attractive proposition. However, there currently is no single noninvasive diagnostic test that is entirely reliable for the evaluation of PH (4).

Transthoracic echocardiography (TTE) is a popular and widely available first-investigation and screening tool for diagnosing PH and estimating pulmonary artery pressure and right ventricle morphology and function. Determination of pulmonary artery pressure commonly involves measuring the peak tricuspid regurgitation velocity and estimating central venous pressure from inferior vena cava compliance. This is calculated by using the modified Bernoulli equation (1) as follows: Pulmonary artery systolic pressure = tricuspid regurgitation pressure gradient ($4 \cdot [\text{tricuspid regurgitation velocity}]^2$) + estimated right atrial pressure (on the basis of inferior vena cava diameter and respiratory variation). Although a linear agreement between noninvasive TTE and invasive RHC pulmonary hemodynamics has been shown, the wide limits of agreement necessitate the use of RHC for definitive initial diagnosis (4). TTE is especially helpful in evaluating left heart function and monitoring PH. However, there are acknowledged limitations in establish-

ing suitable cardiac windows in some patients with interstitial lung disease or emphysema, who are an important potential disease population in PH (12).

Ventilation-perfusion (V/Q) scintigraphy can be used to identify patients with chronic thromboembolic disease and in many centers is still considered an essential planning tool before potentially curative pulmonary artery thromboendarterectomy. Compared with conventional CT or magnetic resonance (MR) imaging, V/Q scintigraphy provides functional information about lung parenchymal perfusion but lacks anatomic resolution (13). MR imaging offers a wide variety of useful indices to evaluate pulmonary perfusion, quantify central flow, assess pulmonary transit time, and evaluate right ventricular function. However, the relatively complex technique, necessity of expert interpretation, and, in some instances, competition for limited MR imaging capacity has limited its applicability to expert centers and established cases of PH. In addition, a major disadvantage of MR imaging as a comprehensive PH imaging solution is its limited use in evaluating the lung parenchyma (14).

Increasingly, CT is routinely used in the evaluation of patients with PH. In established cases, CT is invaluable in helping determine the potential cause of PH or the relative contribution of coexisting pathologic conditions to PH development. Increasingly, CT may be the first investigation to suggest a diagnosis of PH. Several morphologic CT metrics, principally related to the size of the central pulmonary artery vasculature or to right ventricular morphology, have been proposed as indicators of PH and, coupled with the increased use of CT, may contribute to earlier clinical recognition of PH (15). However, the plethora of reported indices of elevated pulmonary artery pressure displays the lack of paired high sensitivity and specificity of these metrics. Such limitations of conventional CT can be partly attributed to the lack of contributory pulmonary perfusion or functional information and may help explain why the contribution of modalities such as V/Q scintigraphy is still regarded as important by many experts in PH.

Teaching Point

The advent of multidetector DECT offers the potential for qualitative and quantitative insights into pulmonary hemodynamics, particularly the distribution of central and peripheral vascular perfusion and the extent and variability of pulmonary parenchymal enhancement. When combined with the morphologic evaluation made possible with multidetector CT, these insights may supply the functional information lacking in conventional single-energy CT studies and increase the clinical utility of CT for evaluation of PH.

DECT for Pulmonary Vascular Imaging

Technology and Principles

Several DECT techniques have been proposed or implemented for use with multidetector CT systems (16,17). These include dual-source systems with separate tubes and corresponding detectors offset at 90° within the z-axis for simultaneous low- and high-kilovoltage image acquisition (18). An alternative system for single-source CT systems makes use of highly responsive detector scintillator materials, which permit rapid kilovoltage switching and double sampling of each ray position at low- and high-kilovoltage spectra (19). Although there are subtle technical differences between these two technologies related to field-of-view availability, image data versus raw data reconstruction, and flexibility of milliamperage alteration, in principle these technologies can generate comparable imaging data and are applicable to DECT pulmonary vascular imaging. Other techniques, such as the use of sandwich detectors to differentiate x-ray spectra (20), have not yet gained wide commercial availability or been investigated for use in pulmonary vascular imaging. The use of a dual sequential acquisition, provided by some single-source manufacturers, is not practical for chest imaging, given the brief period of maximal thoracic vascular enhancement.

DECT produces low- and high-kilovoltage spectra images. These can be combined into weighted-average images that demonstrate optimal noise and contrast characteristics for conventional interpretation. Additionally, material-specific imaging is enabled from the mathematical evaluation of the combination of these datasets. By determining the attenuation of each voxel at low and high kilovoltages and recognizing the attenuation coefficients of expected materials at these specific energies, the contribution to the attenuation of each voxel by three dominant materials can be obtained from a three-material decomposition (21). In turn, the material contribution of any selected calculated material can be added or removed from a projected image or superimposed on a fused image as an overlay (22).

Technique and Image Reconstruction

The images presented in this review were acquired by using a second-generation DECT device (SOMATOM Definition Flash; Siemens Medical Solutions, Forchheim, Germany). Although this system uses two x-ray sources, it is not associated with increased radiation dose levels because the radiation dose is split between the two systems (23).

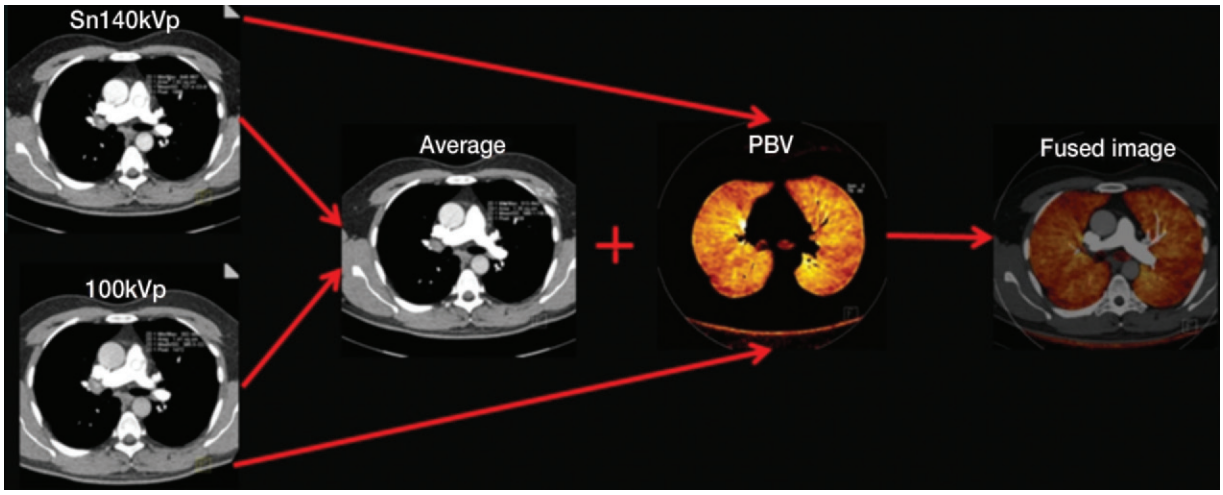

Figure 1. DECT PBV map generation. A PBV map is generated from 100-kVp and Sn 140-kVp images using an algorithm that applies known attenuation-range values for air, soft tissue, and iodine to calculate their relative contribution to each voxel. A Hounsfield-unit thresholding function is used to exclude the central vessels, allowing the PBV map to be overlaid on a weighted-average image to produce a fused PBV image. This enables simultaneous evaluation of the gray-scale vasculature with the color-coded PBV image representing parenchymal perfusion.

The acquisition protocol reflects a minor modification of acute pulmonary embolism imaging protocols as follows: full inspiration; 95–100 mL iohexol contrast agent (iodine, 300 mg/mL) administered at 5 mL/sec with use of an 18-gauge venous access catheter in an antecubital vein, with a 40-mL saline chaser administered at 5 mL/sec; scan delay determined by bolus tracking of a region of interest over the central pulmonary artery (trigger threshold, 100 HU at 120-kVp single-energy acquisition); scan parameters of 100 kVp and tin-filtered (Sn) 140 kVp at effective 150 mAs and 128 mAs, respectively; 128- × 0.6-mm collimation; 0.28-second rotation time; 0.8 pitch; caudocranial acquisition; four-dimensional dose modulation; and coverage from the lung apex to the lung base.

Typical image reconstruction is performed at a 1-mm thickness at 0.8-mm intervals by using a soft convolution algorithm (D30) at 100 kVp and Sn 140 kVp. Principle pulmonary vascular clinical interpretation is performed using a 1-mm, 0.8-mm-interval weighted-average dataset (with 40%:60% weighting from the Sn 140-kVp and 100-kVp images, respectively). This can be supplemented by a review of low-kilovoltage datasets if there is suboptimal vascular opacification of the pulmonary arteries.

Routine material-specific DECT PBV maps can be generated in approximately 30 seconds for an entire thoracic volume on a secondary workstation (Syngo.via Multimodality Workplace; Siemens Medical Solutions). The lung PBV algorithm is used to create a PBV map by using known attenuation range values for air, soft tissue, and iodine at 100 kVp and Sn 140 kVp to calculate their relative contributions to the voxel. A color-coded PBV map is generated that reflects parenchymal enhancement (24).

The algorithm uses a thresholding function to define the volume of lung for analysis, excluding the chest wall, mediastinum, and central larger vessels (default, −960 to −600 HU). For imaging of PH, these default values can be adjusted to include areas of ground-glass opacification that would otherwise be excluded from the analysis. In our practice, the upper range of the default threshold is adjusted to −300 HU to incorporate this analysis. PBV maps can be fused as an overlay on weighted-average images, which permits simultaneous gray-scale evaluation of the enhanced central vasculature and color-coded PBV evaluation of lung parenchymal enhancement (Fig 1).

Perfusion Imaging versus DECT PBV Imaging

True CT perfusion imaging requires multiple image acquisitions at different time points through an area of interest. This enables calculation of an input function and evaluation of the enhancement curve of an area of interest to determine perfusion metrics, including time to peak, mean transit time, PBV, and absolute perfusion (expressed as milliliters per minute per milliliter of tissue). Pulmonary perfusion imaging requires a high-contrast flux with a narrow administration profile that in practice may necessitate flow rates of 8 mL/sec or more. The repeated acquisition of CT datasets, even with adaptations for radiation dose reduction by using low-kilovoltage acquisition or iterative reconstruction, has a punitive effect on the over-

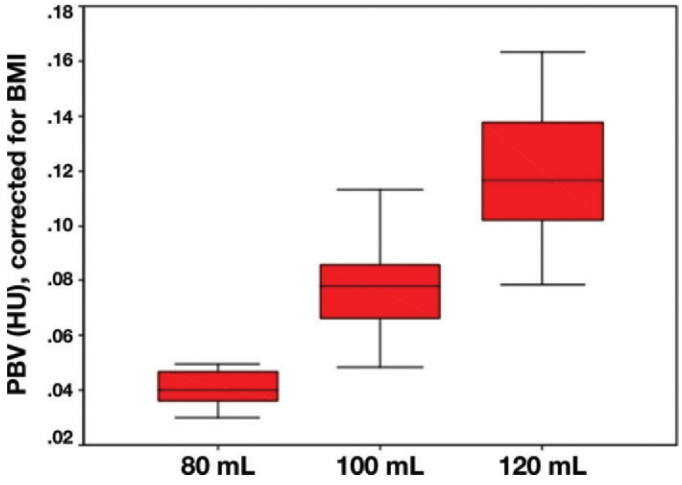

Figure 2. Distribution of PBV-determined enhancement in the lungs of 81 patients (162 lungs). PBV reflects pulmonary vascular enhancement. The box plots show a stepwise increase in lung parenchymal enhancement with increasing volumes of intravenously administered iodinated contrast medium (analysis of variance, $P < .001$), as demonstrated by the increasing volumetrically determined PBV values of each lung (measured in Hounsfield units and corrected for body-mass index *[BMI]*). (Data are from reference 30.)

all patient radiation dose. Because of inevitable respiratory motion, motion-correction software is advisable to reduce misregistration. However, the use of such software does not completely eliminate this artifact. As a result of these limitations, use of the technique has generally been limited to specific areas of the lung parenchyma, principally in patients with focal nodular or mass lesions to help determine malignancy and assess therapy response (25,26). To accommodate perfusion image acquisitions, a dedicated separate study may be required, or the timing of diagnostic imaging of the remainder of the imaged volume may need to be adjusted. The determination of whole-lung perfusion in patients with acute or chronic pulmonary embolic disease has been investigated to a far lesser degree, although there are emerging reports in this area (27).

Teaching Point

PBV imaging is in essence a "two–time-point" perfusion scan. The acquisition time forms the second time point, while the PBV calculation of the iodine content of the lung parenchyma, which can be separated and removed from the inherent physical density of the image, effectively acts as the precontrast initial time point. While such a two–time-point perfusion scan is a reflection of enhancement at only a single point in time and is clearly insufficient to generate the perfusion metrics of a dedicated perfusion scan, PBV imaging nevertheless confers potential advantages. First, the entire lung parenchyma can be easily evaluated without any additional radiation dose. Second, the examination is free of misregistration because the baseline density is calculated from a single acquisition. Finally, there is no interference with the acquisition timing of concomitant CT pulmonary angiography (CTPA) performed to assess the vessels themselves.

Teaching Point

Several studies have demonstrated that PBV imaging can be used to qualitatively assess areas of lung hypoperfusion, in a method similar to scintigraphy (7,28). As a result, PBV imaging is already well established for evaluating acute pulmonary embolism and has an emerging role in PH (29). The accuracy of PBV imaging in determining pulmonary enhancement in humans is difficult to determine because pulmonary dual-energy phantoms do not exist. Experimental comparisons to pre- and postcontrast lung imaging evaluation are limited by motion misregistration. However, indirect evidence that PBV metrics accurately reflect parenchymal enhancement is demonstrated by the stepwise progression of PBV enhancement values of multiple standardized regions of interest on DECT images in healthy patient cohorts examined by using a standard CTPA technique and administering increasing volumes of intravenous contrast agent (30) (Fig 2). Therefore, PBV imaging may justifiably be considered a simplified enhancement surrogate indicator of perfusion.

DECT for Assessment of Pulmonary Embolism and CTEPH

The absolute risk for acute pulmonary embolism progression to CTEPH is unknown and is variably quoted to be between 0.57% and 9.1% (31). Whereas CTPA is the main imaging technique for diagnosis of pulmonary embolism (32), routine rescanning is not warranted because of high radiation exposure. Therefore, there is a clinical need to identify the subset of patients at increased risk for progression to chronic embolic disease. Current CT morphologic measures of thromboembolic clot burden fail to accurately reflect the progression risk.

PBV imaging is well established for depicting areas of hypoperfusion due to acute pulmonary embolism (33–35). However, not all pulmonary emboli are associated with PBV defects (Fig 3). In a study of 117 patients (17 with pulmonary embolism), only five of 58 patients with a nonocclusive

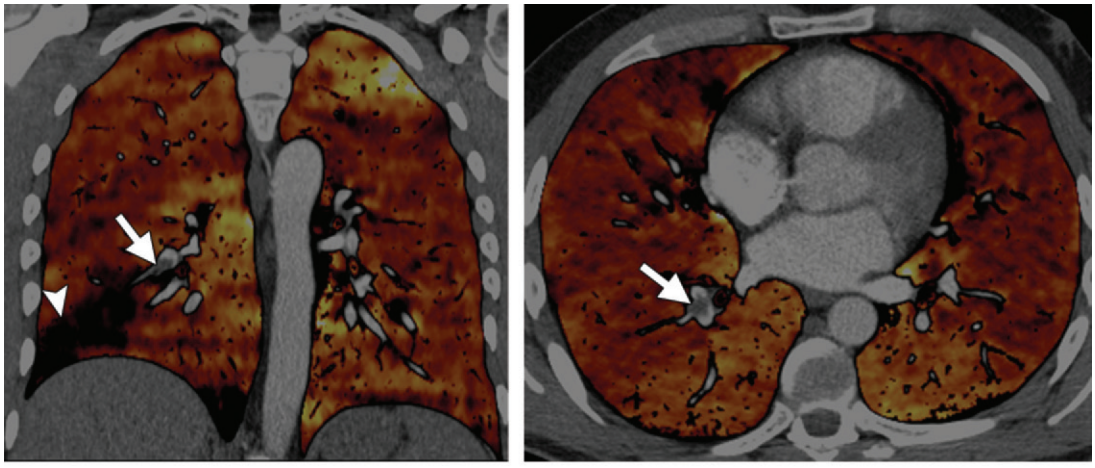

a. b.

Figure 3. Differentiation of embolic physiologic characteristics in a 49-year-old woman who presented with acute pulmonary embolism. **(a)** Coronal color-coded PBV image shows an occlusive right lower lobe lateral pulmonary artery embolism (arrow) and corresponding perfusion defect (arrowhead). **(b)** Axial PBV image shows nonocclusive pulmonary emboli in the posterior right lower lobe (arrow) that are not associated with PBV defects. Differentiation of occlusive from nonocclusive emboli could be inferred without PBV imaging on multiple vessel–aligned multiplanar reconstructions, but the PBV images directly demonstrate the peripheral physiologic effect.

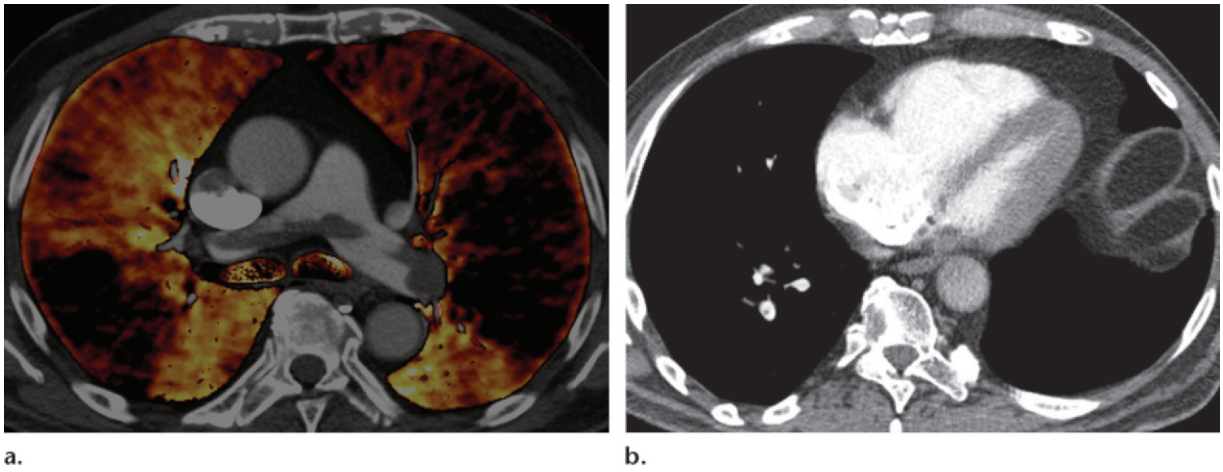

a. b.

Figure 4. Correlation of perfusion defect size with pulmonary embolism severity in a 55-year-old man who presented with collapse. **(a)** Axial fused PBV image shows a saddle embolus with extensive bilateral perfusion defects. **(b)** Axial mixed (100-kVp and Sn 140-kVp) DECT image shows an enlarged right-to-left ventricular ratio and posterior deviation of the interventricular septum, findings consistent with a massive pulmonary embolus.

pulmonary embolism had PBV defects (34). In a comparable study of 93 patients (23 with pulmonary embolism), only two of 33 patients with nonocclusive emboli had PBV defects (36). However, in both studies, the rate of PBV defects in patients with an occlusive pulmonary embolism was far higher (14 of 17 patients and 42 of 44 patients, respectively). Other studies have demonstrated that the overall extent of perfusion defects correlates with endoluminal clot burden (determined by the Qanadli or Mastora indices) and right heart strain (indicated by increased right-to-left ventricular ratios) (37,38) (Fig 4). In addition, PBV defects are positively correlated with troponin I levels and inversely related to arterial oxygen (PaO_2) levels, which further reinforces the principle that PBV defects appear to reflect more physiologically impairing embolic disease (39). The prognostic value of PBV imaging defects in impaired physiology is reflected in a study by Bauer et al (10), who found that re-presentation or death from acute pulmonary embolism occurred only in patients with a perfusion defect volume greater than 5% relative to total lung volume. The median survival time was significantly shorter for these patients.

Although a growing body of data suggests a potential role for quantification of DECT-derived perfusion defects in the prognostication

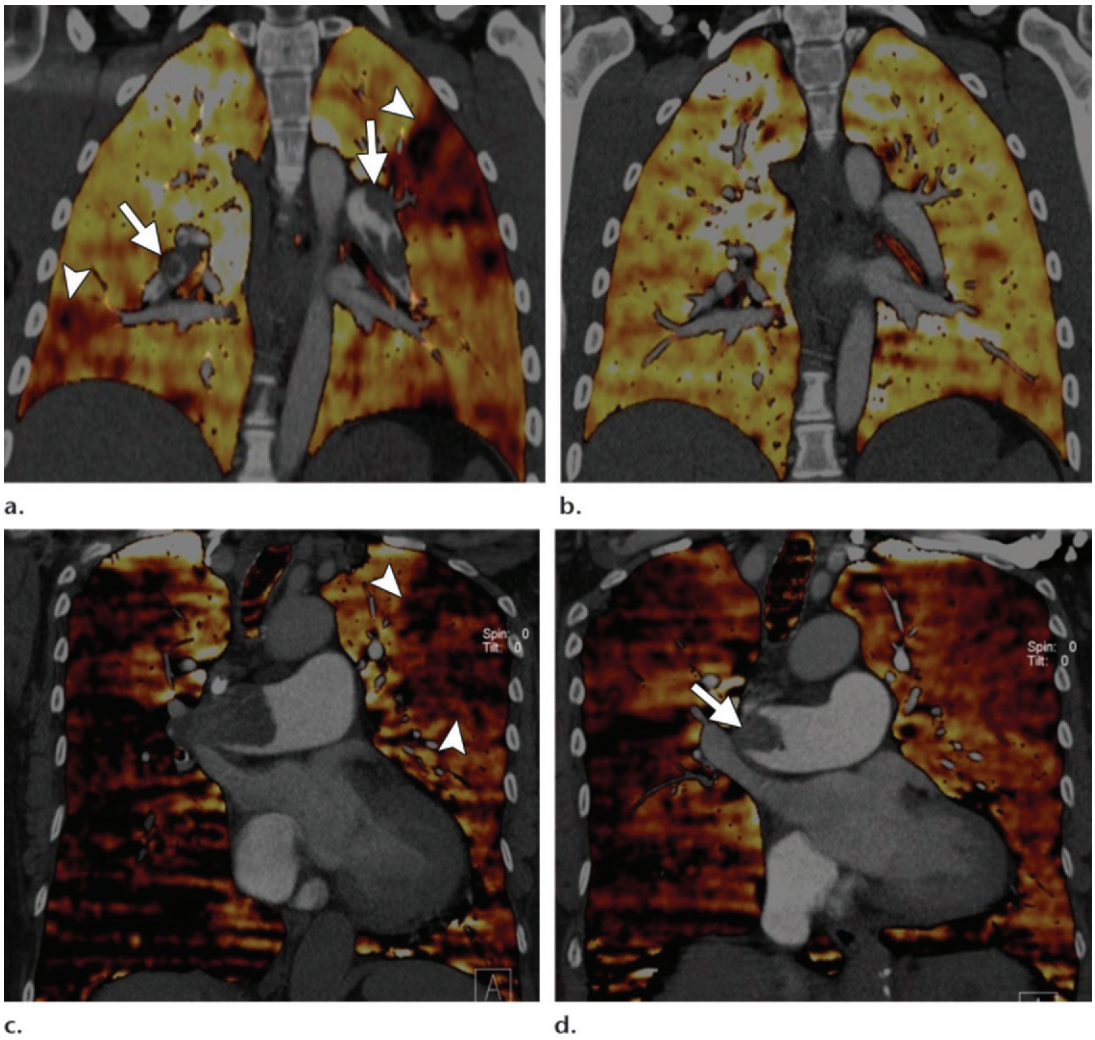

Figure 5. Pulmonary embolism follow-up and risk for progression to CTEPH in two patients. **(a, b)** A 45-year-old woman who presented with acute shortness of breath. **(a)** Coronal fused PBV image obtained at presentation shows bilateral emboli (arrows) with corresponding perfusion defects (arrowheads). However, the overall perfusion-defect volume is not large, and no right ventricular dysfunction was seen at echocardiography. **(b)** Coronal fused PBV image obtained after 4 months of anticoagulation therapy (without thrombolysis) shows resolution of the clots and normal lung perfusion. **(c, d)** A 67-year-old woman who presented with collapse. **(c)** Coronal fused PBV image obtained at presentation shows a large occlusive thrombus in the right main pulmonary artery, with marked patchy reduced perfusion in the right lung and a smaller wedge-shaped defect in the left upper lobe (arrowheads). Despite anticoagulation therapy and thrombolysis, the patient had progressive symptoms of right heart failure, with raised pulmonary artery pressure seen at echocardiography. **(d)** Coronal fused PBV image obtained 7 months later confirms clinical progression and shows features of CTEPH, with clot retraction (arrow) and large residual perfusion defects.

of pulmonary embolism, (40,41), the added value of this measure compared with conventional CT measures of cardiac strain and standard laboratory markers is unsubstantiated but is the subject of ongoing evaluation. It is reasonable to suggest that the extent of PBV defects, in combination with other clinical parameters (eg, thrombophilia, extent of pulmonary embolism, and right ventricular dysfunction), may help determine the need for follow-up imaging and perhaps the risk for progression to CTEPH (Fig 5). However, there is no direct prospective evidence that PBV defects predict the evolution of CTEPH.

At our institution, we aim to use DECT for all patients with suspected pulmonary embolism or PH. Exceptions include patients who are very obese (particularly relevant when using first-generation dual-source scanners with a limited field of view and greater noise on low-kilovoltage images); patients with severe tachypnea (where a high-pitch protocol is more appropriate); and patients for whom the radiation dose is critical (eg, pediatric or pregnant patients), where a

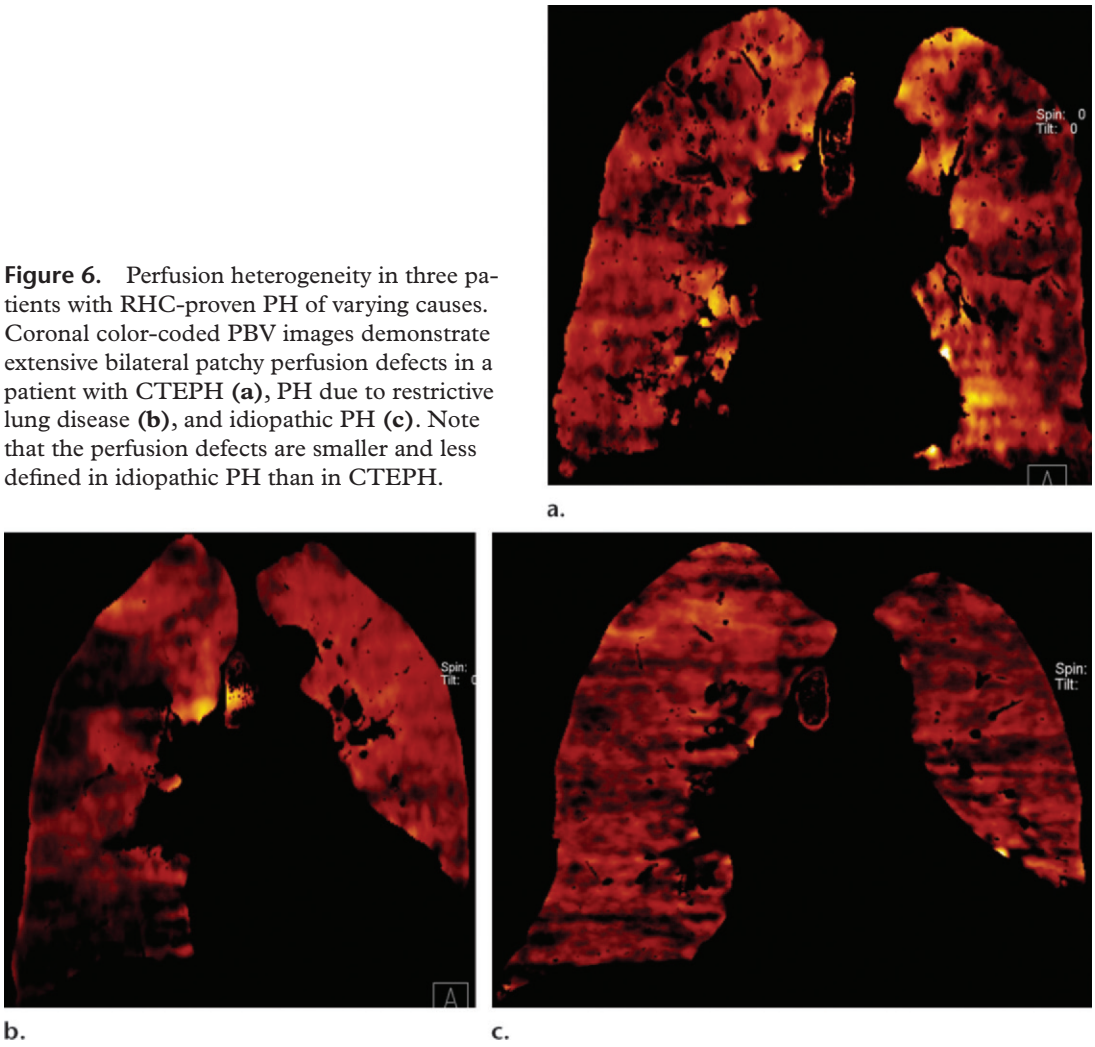

Figure 6. Perfusion heterogeneity in three patients with RHC-proven PH of varying causes. Coronal color-coded PBV images demonstrate extensive bilateral patchy perfusion defects in a patient with CTEPH **(a)**, PH due to restrictive lung disease **(b)**, and idiopathic PH **(c)**. Note that the perfusion defects are smaller and less defined in idiopathic PH than in CTEPH.

single-energy lower-radiation-dose protocol may be achievable.

Perfusion Imaging in PH

Perfusion defects seen in CTEPH, and more widely in PH, are in general analogous to but more pronounced than those seen in acute pulmonary embolism (Fig 6). The presence and significance of perfusion abnormalities in patients with PH have been most widely evaluated in those with CTEPH (42–46). Differentiation of this cohort from patients with nonembolic PH is important, as patients with CTEPH represent a distinct category with potentially curable disease by use of pulmonary thromboendarterectomy. Untreated CTEPH carries a poor prognosis, with a 5-year survival rate of 30% (47).

The pathophysiology of CTEPH is poorly understood but in part relates to the incomplete resolution of endovascular thromboembolic material, which is remodeled into intravascular scars that result in stenosis or obstruction of the pulmonary arteries (48). The presence of consequent perfusion heterogeneity, first described at planar scintigraphy (49) and more recently observed at PBV imaging, is well recognized in this condition. Furthermore, at PBV imaging analysis of CTEPH cases, the most severe pulmonary arterial features of CTEPH, including webs, bands, focal stenosis, and occlusion, are seen more frequently in segments with perfusion defects than in those with normal perfusion (45) (Fig 7).

Teaching Point

In clinical practice, patients with CTEPH may present with various indications for imaging, such as follow-up of prior pulmonary embolic disease, exclusion of acute pulmonary embolism, or investigation of chronic hypoxia or known PH. Conventional CTPA can elegantly demonstrate endovascular thrombi and provide other morphologic information, including mosaic lung changes and structural information on right ventricular configuration (50). However, conventional CTPA does not provide functional information about parenchymal perfusion, and it has been reported that peripheral subsegmental thrombi may be poorly visualized. A study by Pitton et al (51)

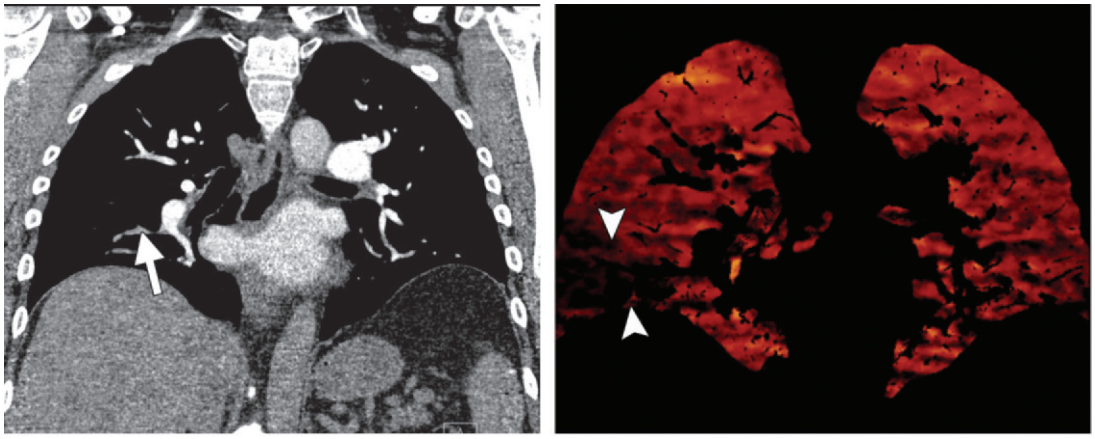

a. b.

Figure 7. Concordance of pulmonary arterial features of CTEPH with areas of perfusion defects in a 65-year-old man. **(a)** Coronal mixed (100-kVp and Sn 140-kVp) CTPA image shows a serpiginous right lower lobe segmental artery with focal stenosis and occlusion (arrow). **(b)** Coronal color-coded PBV image shows a predominant right lower perfusion defect (arrowheads) that corresponds to the area with the most marked vascular features of CTEPH seen in **a**.

suggests a sensitivity of 64%–70% for multidetector CTPA compared with selective pulmonary digital subtraction angiography for detection of segmental and subsegmental chronic thromboembolic disease. A different retrospective single-center review of 227 patients with PH reported a sensitivity of 51% for detection of CTEPH with multidetector CTPA, versus a 97% sensitivity with V/Q scintigraphy (52).

Such analyses are not infrequently biased by the difficulty of determining an independent criterion standard for the ultimate diagnosis of CTEPH or by the extent of vessel involvement. High-probability V/Q scans or individual perfusion defects in patients are often assumed to be due to CTEPH, although such defects in patients with PH may not be exclusively related to CTEPH (49,53). Traditional research study criterion-standard corroboration with selective pulmonary digital subtraction angiography should also be considered potentially deficient in light of interobserver variability in interpretation and the recognition that many causes of PH may have similar end results on the morphology of peripheral arteries. In addition, digital subtraction angiography is expensive and invasive, with increased risk in patients with PH. Combined with the lack of functional information generated with conventional CTPA, these factors help explain the continued importance ascribed to V/Q scintigraphy in evaluating patients with CTEPH.

If DECT can provide functional perfusion information comparable to that of V/Q scintigraphy, then it is possible to envisage this technique as a single diagnostic and preoperative planning study for patients with CTEPH, combining high anatomic resolution for vessel evaluation with a functional imaging display (at a resolution that exceeds that of V/Q scintigraphy or even single photon emission CT [SPECT] imaging). Compared with single-energy CTPA, perfusion information from PBV imaging may also more accurately reflect overall pulmonary vascular reserve and parenchymal arterial perfusion, including pulmonary artery and bronchial arterial supply.

DECT Correlation with Scintigraphy

To date there have been limited studies assessing the correlation between pulmonary embolism–related perfusion defects seen at DECT and those seen at V/Q scintigraphy (54) and SPECT (55). Thieme et al (54) reported limited diagnostic accuracy for PBV maps, with 75% sensitivity and 80% specificity for pulmonary embolism in a per-patient analysis, but these increased to 83% and 99% in a per-segment analysis. DECT PBV perfusion defects related to SPECT imaging had a sensitivity of 77% and a specificity of 98% in a follow-up study by the same group (55). A complete concordance between defects seen at DECT PBV imaging and scintigraphy is unlikely. Not only are these measures not precisely physiologically equivalent, but V/Q scintigraphy is performed during shallow respiration, whereas DECT PBV maps reflect full inspiration. The degree of agreement between DECT PBV and scintigraphic images is encouraging, particularly on a clinically significant per-segment basis.

Nakazawa et al (43) analyzed PBV imaging correlation with SPECT in 51 patients and found PBV imaging to have a sensitivity of 96% and a specificity of 76%. The relatively low specificity was attributed to streak artifact due to high-density contrast material in the venous system

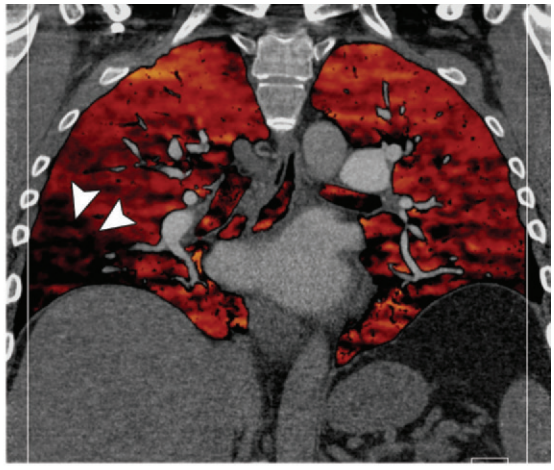

a.

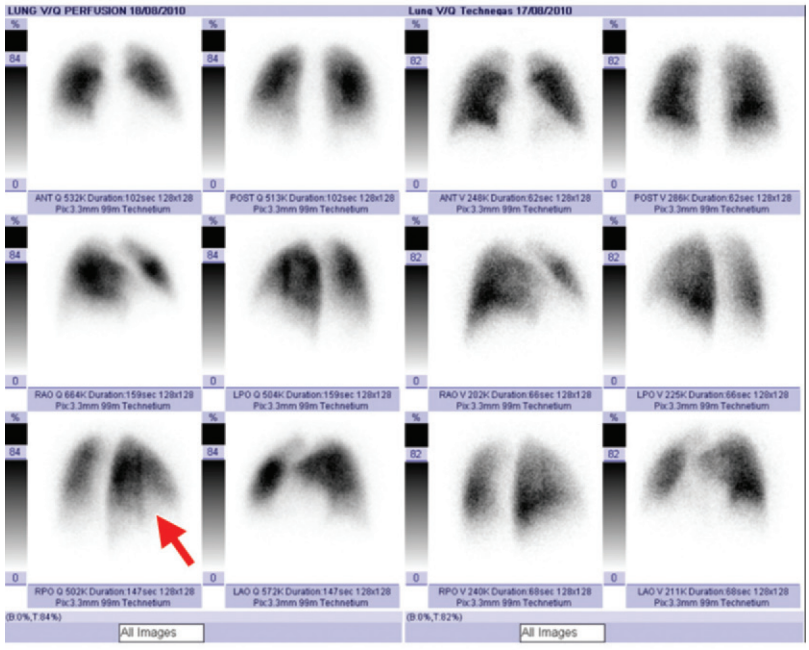

b.

Figure 8. Correlation of PBV imaging with V/Q scintigraphy in the same patient as in Figure 7. **(a)** Coronal fused PBV image shows right lower lobe emboli and a corresponding focal perfusion defect in the right lower lobe (arrowheads). **(b)** V/Q scintigram shows subsegmental areas of V/Q mismatch at the right base, which are best demonstrated on a right posterior oblique image (red arrow).

and the excellent sensitivity to the higher contrast and spatial resolution of CT versus scintigraphy. This enabled identification of smaller areas of hypoperfusion at CT that were not detected at scintigraphy. The authors conclude that PBV imaging is representative of lung perfusion and is comparable to scintigraphy for evaluating pulmonary perfusion in CTEPH (Figs 8, 9).

Teaching Point

The combined intravascular and parenchymal enhancement information available at dual-energy CTPA with PBV imaging can also be used to determine whether areas of perfusion defect correspond to focal vascular obstruction, and consequently to determine the optimal therapeutic strategy. Current surgical data suggest that in cases of perfusion defects with a visualized vascular obstruction correlate, surgery is more likely to be successful; conversely, when no focal vascular obstruction is identified as the cause of a perfusion defect, raised pulmonary pressure and increased pulmonary vascular resistance are likely to be sustained after surgical intervention and result in a higher complication rate (56,57). Therefore, DECT with PBV mapping may aid in reducing the increased morbidity and mortality of patients with isolated peripheral CTEPH, which is characterized by V/Q perfusion defects and CT-depicted vascular mosaic attenuation but the absence of an overt intraluminal clot at CTPA. An integrated DECT approach that combines the higher anatomic resolution of PBV imaging with simultaneous CTPA for vascular evaluation may potentially be advantageous versus a sequential approach of V/Q scintigraphy and conventional CTPA.

The presence of matched ventilation and perfusion defects can be a confounder in the scintigraphic evaluation of patients with CTEPH or

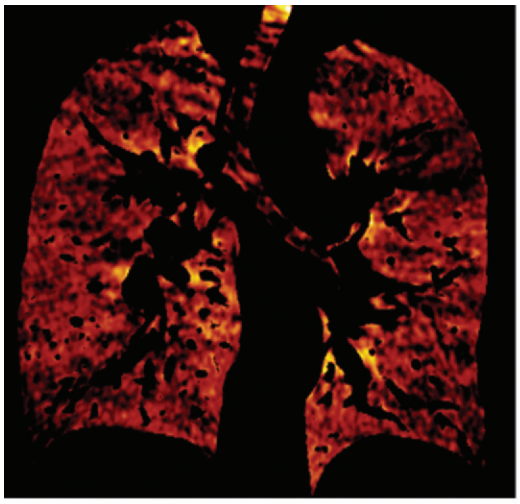

a.

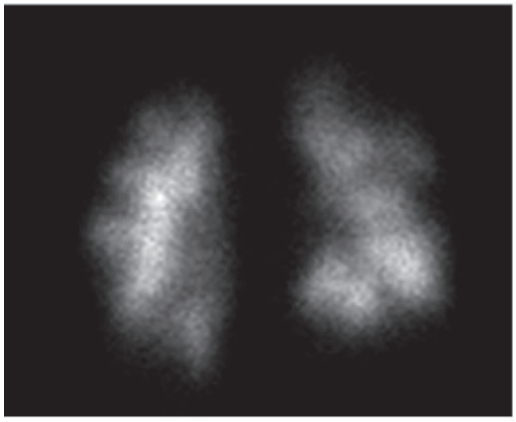

b.

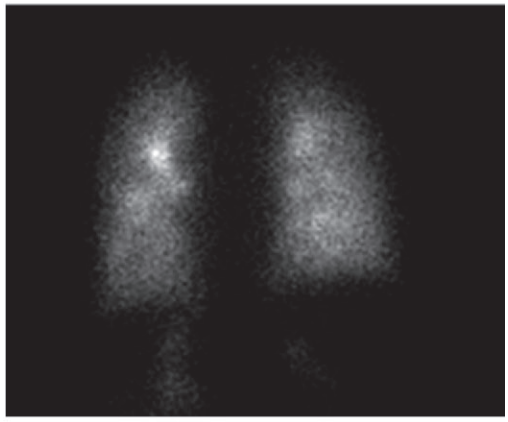

c.

Figure 9. Correlation of PBV imaging with SPECT in a 59-year-old man with CTEPH. **(a)** Coronal color-coded PBV image shows heterogeneous perfusion of the lungs, with bilateral patchy perfusion defects. **(b)** Corresponding coronal SPECT image shows comparable patchy perfusion defects. **(c)** Planar scintigraphic ventilation image shows preserved ventilation in both lungs.

PH. It may be impossible to determine whether these areas reflect a chronic physiologic response to vascular occlusion or concurrent obstructive airways disease that is coincidental to or the cause of PH. PBV defects seen at DECT can be correlated to anatomic vascular changes to help determine their significance. It also is possible with DECT to generate ventilation images by using inhaled high-density gases such as xenon, which has x-ray absorption characteristics similar to those of iodine. DECT is used to produce maps of regional lung ventilation. The limited availability of xenon gas and the required careful monitoring of its anesthetic properties have limited this type of investigation to feasibility studies as a surrogate for full-ventilation scintigraphy with DECT (58).

Microvascular Assessment: Beyond CTPA and Scintigraphic Resolution

The axial resolution of isotropic multidetector CT images approaches 0.5–0.6 mm with many current systems, although confident detection of acute or chronic intraluminal filling defects can realistically be made only in vessels measuring 2 mm or more. The resolution of scintigraphy (7–8 mm), even when aided by SPECT (3–4 mm), is considerably lower, although there is no strict anatomic correlate in V/Q scintigraphy. Hence it is possible that small perfusion defects may be present at lung parenchymal imaging, where the patency of the subtending vessel is too small to evaluate with current imaging methodologies (including state-of-the-art multidetector CT with CTPA). Such small PBV defects are occasionally seen in patients with CTEPH and possibly reflect perfusion defects below the resolution limits of multidetector CT with CTPA (Fig 10).

There is an established basis for suspecting that these defects reflect small vascular CTEPH perfusion defects. In proven cases of acute pulmonary embolism, perfusion defects are occasionally seen in the absence of a visible embolus in the supplying pulmonary arteries. Thieme et al (55) reported two cases of corresponding perfusion defects seen at both scintigraphy and DECT PBV imaging with no visualized embolus seen on CTPA weighted-average images. They proposed that the observed perfusion defects probably corresponded to segments of prior pulmonary

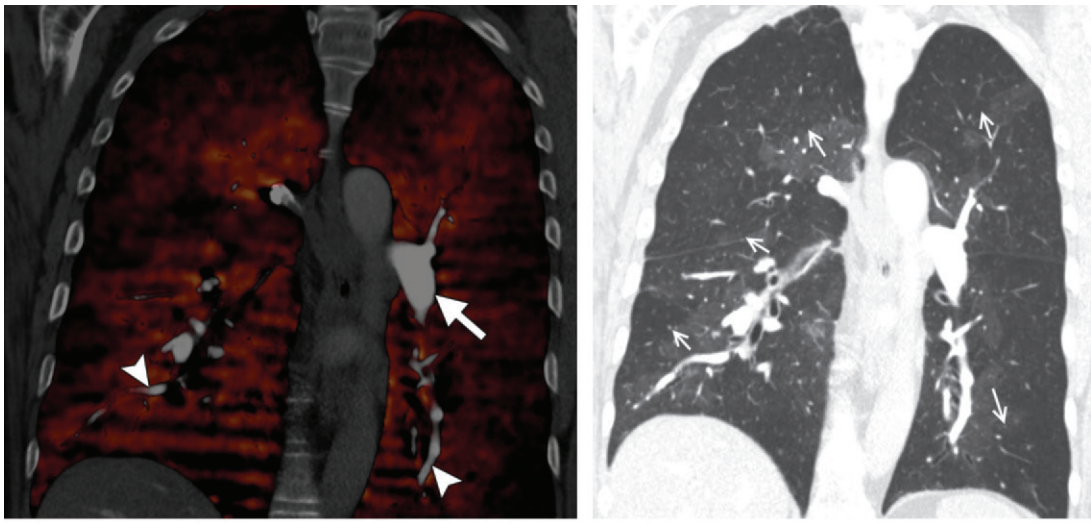

a. b.

Figure 10. Peripheral perfusion defects beyond the resolution of CTPA in a 73-year-old woman with CTEPH. **(a)** Coronal fused PBV image shows several small peripheral perfusion defects at both lung bases, including very small defects at the right lung base that would be beyond the resolution of perfusion scintigraphy. Note the absence of filling defects in the central (arrow) and peripheral (arrowheads) pulmonary arteries. This likely reflects perfusion defects beyond the resolution of CTPA. **(b)** Coronal mixed (100-kVp and Sn 140-kVp) lung-window image shows bilateral mosaic lung attenuation (MLA), with areas of reduced attenuation (arrows) that closely reflect the perfusion defects seen on the PBV image.

embolism with reperfused segmental vessels and residual peripheral thrombosed vessels, which are too small to visualize at multidetector CT with CTPA. Similarly, Pontana et al (35) found four subsegmental perfusion defects with no visualized embolus in 17 patients with confirmed pulmonary embolism.

In clinical practice, these small peripheral defects are not uncommon in patients with acute pulmonary embolic disease and appear in areas with no overt occlusive vascular changes. They are usually triangular and peripheral and cannot be accounted for by overt artifacts. In contradistinction to the long-standing nature of such small defects in CTEPH, these small defects in acute pulmonary embolic disease tend to resolve with anticoagulation therapy, paralleling the resolution of other defects (Fig 11). While the significance of these findings requires further investigation, PBV imaging may potentially increase the sensitivity for detection of peripheral microemboli beyond the resolution of current CT and scintigraphic techniques. This may be of particular importance in patients with CTEPH and microvascular involvement.

DECT for Assessment of MLA

The variability of lung parenchymal perfusion in PH may be better reflected by considering the presence of MLA, defined as geographic areas of variable lung attenuation seen on thin-section CT images. In MLA of vascular origin, higher-attenuation areas correspond to normal or hyperperfused lung and may demonstrate increased vascular size, whereas darker areas are often accompanied by diminutive vessel size and correspond to regions of hypoperfusion (59). Whereas airway disease can also result in MLA, true MLA in airway disease is also contributed to by air trapping. Vascular perfusion in airway disease is also likely reduced by secondary autoregulation. However, in practice, there is less morphologic vascular size variation in airway disease, and vascular perfusion reduction may be less marked.

The concordance of MLA and variable perfusion has been investigated by correlating the findings of single-energy CT and scintigraphy. Rossi et al (59) and Bartalena et al (53) have demonstrated high concordance between mosaic changes, which were accentuated on minimum intensity projection images, and perfusion abnormalities at scintigraphy. It is hypothesized that at DECT, concordant PBV perfusion defects and hypoattenuating areas of MLA indicate a vascular cause for MLA, whereas discordance suggests air trapping due to airway-predominant disease (Fig 12). A strong correlation between the extent of hypoperfusion at DECT PBV imaging and MLA has been demonstrated in a cohort of 20 patients with CTEPH (42) (Fig 10). Moreover, Pontana et al (60) studied patients with chronic obstructive pulmonary disease and determined that DECT could depict ground-glass attenuation of vascular origin by means of the higher iodine content in these segments.

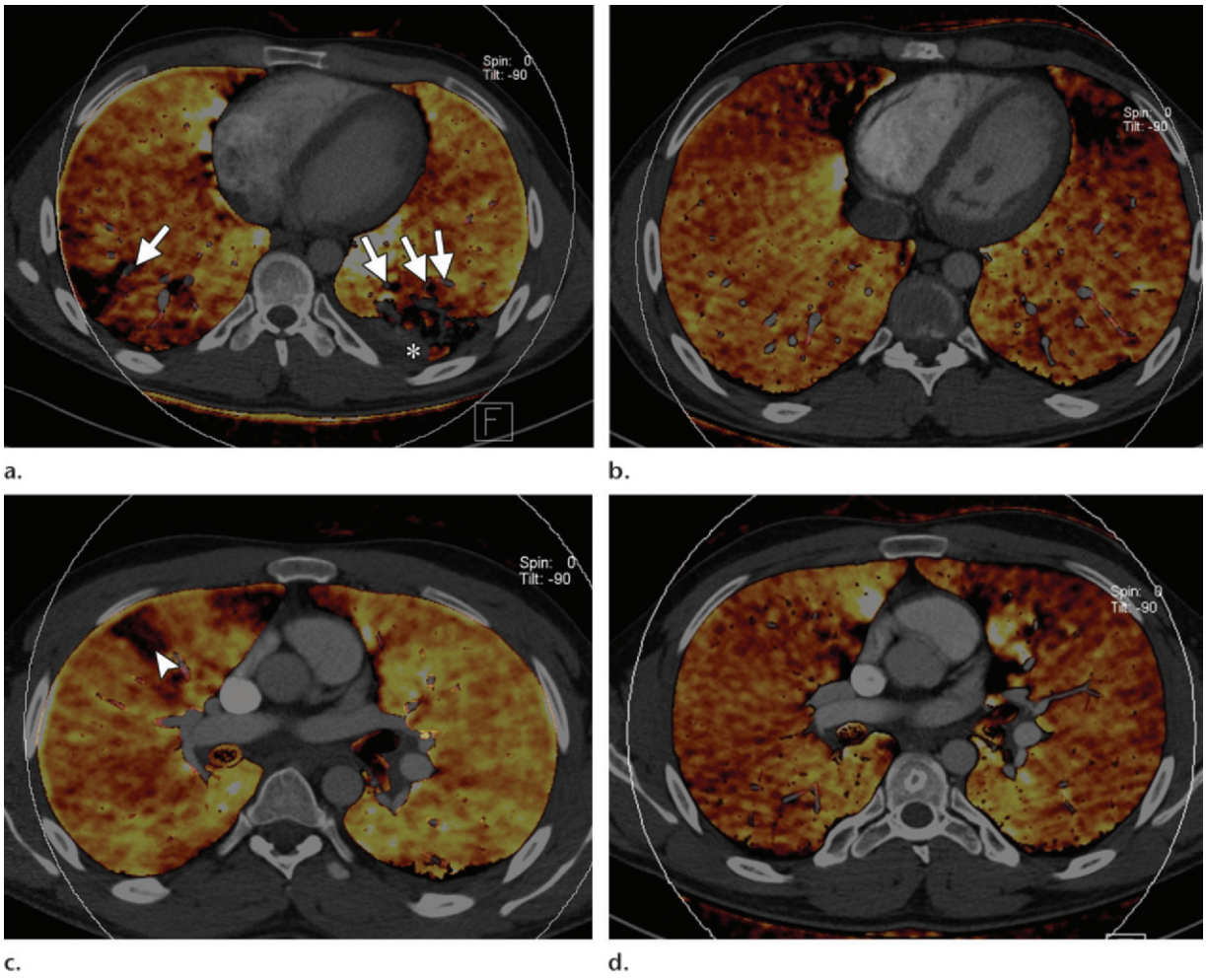

Figure 11. Segmental perfusion defects in a 45-year-old woman with a pulmonary embolism. **(a)** Axial fused PBV image obtained at presentation shows bilateral lower lobe perfusion defects due to occlusive pulmonary emboli (arrows), with associated PBV defects. Note the left basal atelectasis (*). **(b)** Axial fused PBV image obtained after 6 months of anticoagulation therapy shows resolution of the intraluminal clots and normal perfusion. Note the cardiac motion artifact in the middle lobe and lingula. **(c)** Axial fused PBV image obtained at presentation shows a wedge-shaped peripheral area of perfusion defect (arrowhead) that does not correspond to any known artifact or parenchymal abnormality. However, no endovascular embolus is visible. **(d)** Axial fused PBV image obtained after anticoagulation treatment shows defect resolution.

These results suggest that in patients with PH who also have CTEPH, DECT PBV imaging may be helpful in further subcategorizing the heterogeneous group of patients with numerous lobes with mosaic attenuation at initial imaging. These mosaic changes have been postulated to reflect extensive distal disease and may indicate an adverse prognosis for endarterectomy (61).

Increasingly, there is recognition by PH imaging centers that MLA, although more common and more marked in CTEPH, is also a feature of non-CTEPH causes of PH. This is likely due to focal under- and overperfusion from the structural pulmonary vascular changes that occur in PH, which include various degrees of vascular endothelial damage, cellular proliferation, and vasoconstriction and occlusion in the distal pulmonary vasculature, a common end pathway of many disease processes. Perfusion inhomogeneities at DECT PBV imaging of patients with PH are also common, are seen in most cases, and are not limited to CTEPH. Findings of perfusion heterogeneity in non-CTEPH cases mirror observations at scintigraphy. Although in PH, high-probability V/Q scan results are usually assigned to a CTEPH cause, perfusion abnormalities related to other causes of PH have long been recognized and often are referred to as having a "mottled" pattern (49). Talwar et al (62) exploited this variability finding and demonstrated a high correlation between PVR and a scintigraphically derived perfusion index in patients with pulmonary arterial hypertension without pulmonary embolism.

Animal model studies have confirmed that the variability of pulmonary perfusion at DECT

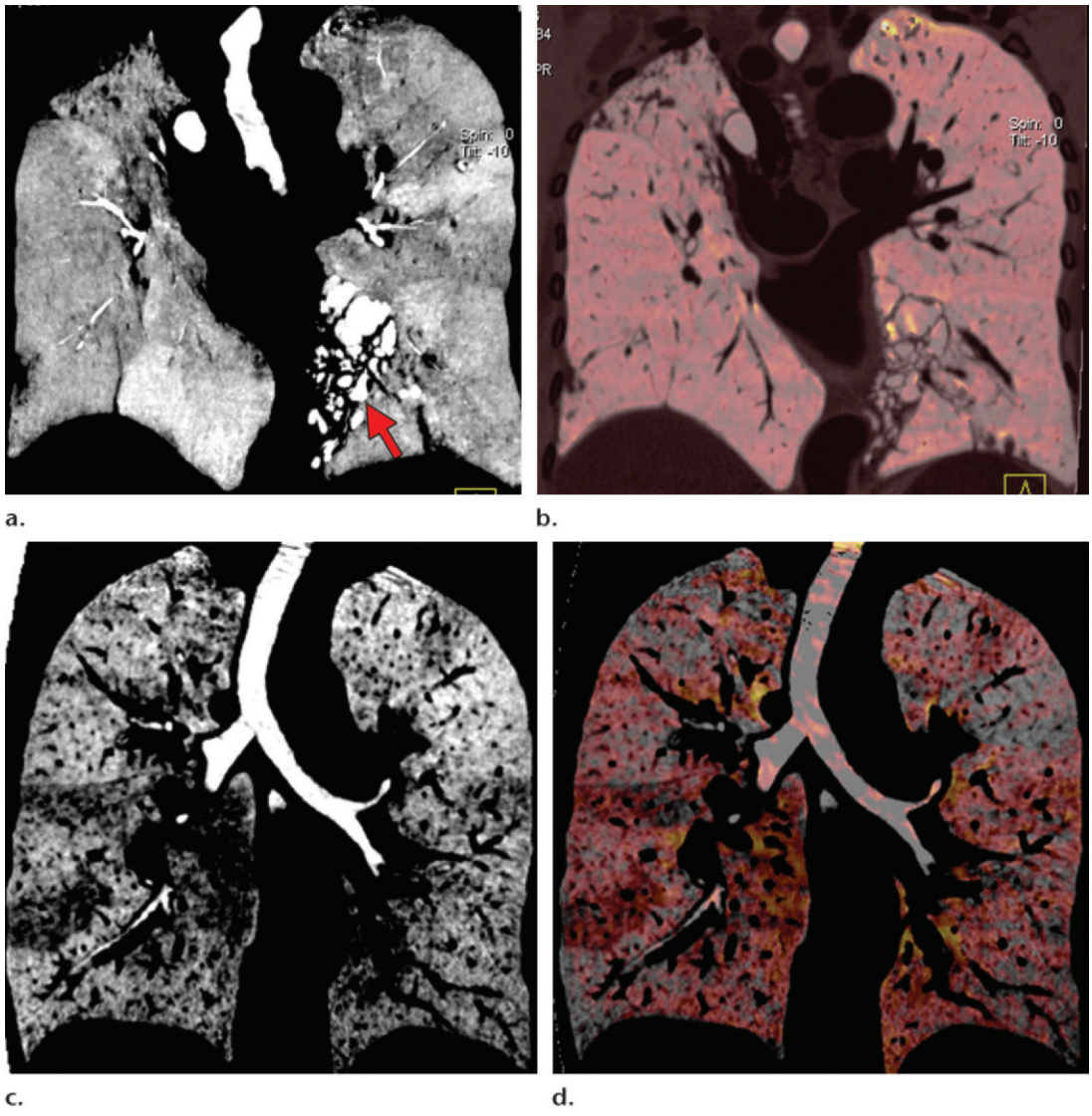

Figure 12. DECT used to differentiate causes of mosaicism in two patients. Inverted gray-scale images were created by subtracting low-kilovoltage images from weighted-average images. This results in images in which contrast has been effectively removed, thereby highlighting mosaicism. The inverted gray scale permits superimposition with PBV images. **(a, b)** Images show mismatched attenuation-perfusion defects in a 39-year-old man with bronchiectasis. **(a)** Coronal inverted gray-scale image shows an area of bronchiectasis (red arrow) in the left lower lobe and diffuse MLA due to air trapping. The white areas indicate reduced attenuation. **(b)** Coronal PBV overlay image shows preserved homogeneous bilateral lung perfusion. **(c, d)** Images show matched attenuation-perfusion defects in a 58-year-old man with CTEPH. **(c)** Coronal inverted gray-scale image shows heterogeneous lung attenuation due to vascular MLA. **(d)** Coronal PBV image confirms patchy lung perfusion, with the areas of perfusion defect closely matching the areas of MLA-related hypoattenuation seen in **c**.

PBV imaging accurately reflects variations in pulmonary perfused blood volume (63). Recent research on humans also demonstrates that the regional variability of PBV measurements (performed either by manual placement of standardized multiple two-dimensional regions of interest or by regional automated volumetric PBV measures) shows a strong correlation with PVR in patients with a wide variety of PH causes (64).

Because DECT with CTPA can combine morphologic pulmonary vascular imaging, high-resolution multidetector CT lung imaging, and PBV characterization of lung parenchymal enhancement, the technique provides the potential for a powerful "one-stop" investigation of PH. The emerging data suggest that PBV imaging may be an accurate and sensitive indicator of PH perfusion variability. This better depiction of subtle lung density and perfusion variation relates to the improved contrast resolution of low kilovoltage images and the accentuation of regional parenchymal enhancement differences on PBV maps.

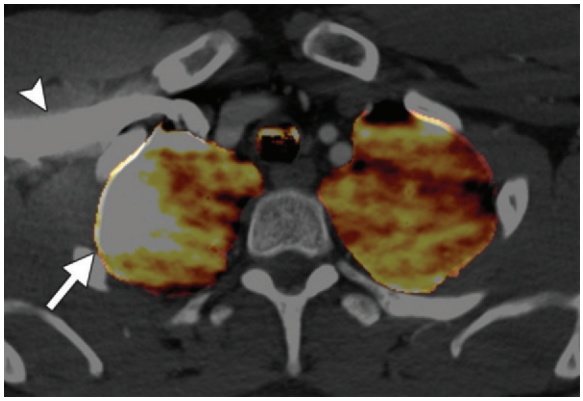

Figure 13. Artifactual perfusion defects in the absence of pulmonary emboli or PH. Axial fused mixed-kilovoltage and PBV image demonstrates windmill (beam-hardening) artifacts (arrow) due to high-density contrast material in the subclavian vein (arrowhead).

The potential benefit of PBV imaging variation to reflect PVR is of critical importance. Although most prior attempts to correlate morphologic CT features with right heart function have focused on mean pulmonary artery pressure, PVR is arguably more important, particularly as a true determinant of pulmonary vascular disease that can guide pulmonary vasodilator therapy. This is because as PVR rises, eventual heart failure may result in cardiac output reduction paralleled by a fall in mean pulmonary artery pressure. Therefore, the reduction in mean pulmonary artery pressure under these circumstances is a paradoxically adverse outcome. Because many newer vasodilator therapies are expensive but do not work in all patients, it is possible that PBV variability metrics may assist in differentiating early vasodilator responders from nonresponders.

PBV findings in PH are best described for CTEPH, perhaps in part because of the more marked mosaic attenuation in CTEPH. There currently is no evidence that PBV maps can add to conventional CTPA images to help differentiate causes of PH. However, subtle differences in the appearances of PBV images are observable at DECT, paralleling observations from V/Q scintigraphic studies that use scintigraphic patterns to discern CTEPH and idiopathic pulmonary arterial hypertension (49). PBV defects that reflect perfusion defects in patients with CTEPH are typically multiple, segmental, and sharply defined, while in patients with idiopathic pulmonary arterial hypertension, these defects are more typically nonsegmental, patchy, and inhomogeneous in distribution, often without discrete defects (Fig 6).

Pseudodefects: Nonembolic Perfusion Defects

Although PBV defects appear to have physiologic significance in both acute pulmonary embolic disease and PH, not all perfusion defects reflect true parenchymal hypoperfusion. Artifacts, or pseudodefects, seen at DECT PBV imaging are not uncommon and require familiarity with their appearance and causes. Such pseudodefects are most frequently caused by motion artifact or contrast material–related beam hardening. A study of 48 DECT scans in patients without embolic disease demonstrated 212 perfusion defects, 202 of which were accounted for by motion and beam-hardening artifacts (65). Recognition of pseudodefects is important to avoid erroneous interpretation.

Motion artifact is typically due to cardiac and respiratory motion and is seen as a linear or crescent area of perfusion defects adjacent to the heart border or hemidiaphragms. It can be confirmed by observing blurring in the corresponding lung window. Appropriate breath-holding instructions and electrocardiographic gating can help minimize motion artifacts (9).

High-density contrast material in the central vessels commonly results in "windmill" (beam-hardening) artifacts, which are typically seen adjacent to the right atrium, superior vena cava, and subclavian vein and follow the peak contrast material density (Fig 13). These can be minimized by scanning in a caudocranial direction (8), using a saline flush, and administering a lower volume of contrast agent with slightly later image acquisition. Both latter factors are possible at DECT with CTPA, given the inherent improved iodine-enhanced image contrast on associated low-kilovoltage images.

An underrecognized cause of "out-of-range" pseudodefects results from the thresholding function, which defines the range of included attenuations in the PBV calculation. Voxels with Hounsfield unit values outside of the range are assigned a value of 0 and are displayed as black on the PBV image. These areas then mimic areas of genuine perfusion defects in qualitative evaluation or as part of a region of interest for quantitative evaluation. These defects are particularly important in patients with PH, who have a high

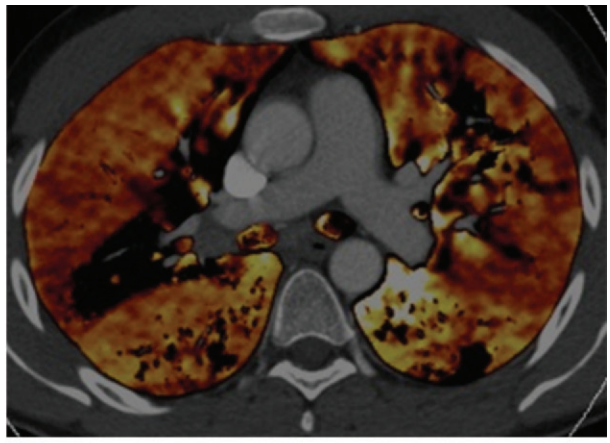

a.

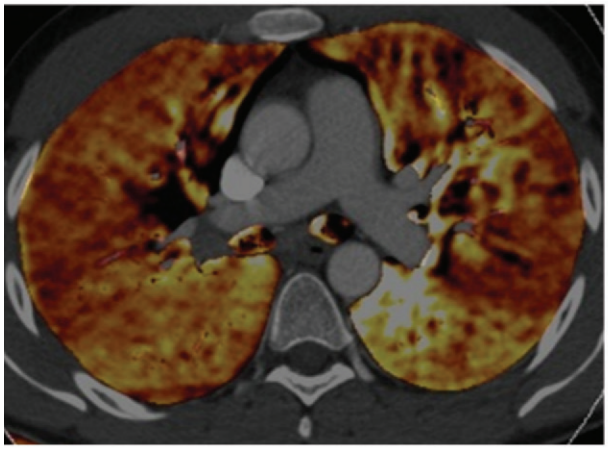

b.

c.

Figure 14. Out-of-range perfusion defects in a 53-year-old male patient with biventricular failure. **(a)** Axial PBV image (maximum threshold set at −600 HU) shows bilateral areas of apparent perfusion defects. **(b)** Axial PBV image (maximum threshold changed to −300 HU) shows a reduced size of the "defects" and demonstrates that many of these areas are actually well perfused. **(c)** Axial lung-window image shows bilateral dependent patchy areas of ground-glass attenuation, which correspond to the areas of perfusion pseudodefects seen in **a** with the low maximum-threshold setting.

prevalence of ground-glass attenuation and emphysema. Increasing the range of the minimum and maximum thresholds will depict iodine concentration in tissues of a wider density (Fig 14).

Other DECT Applications in PH

Low-Kilovoltage Image Availability

Increased photoelectric interactions at 100 kVp compared with at 140 kVp and the relative proximity of the iodine k-edge (33 KeV) result in greater iodine conspicuity on lower-kilovoltage images. This conspicuity allows better visualization of the peripheral arteries and potentially salvages studies with suboptimal pulmonary arterial enhancement (22). Such visualization may be particularly advantageous in cases of PH with poor cardiac function. The increased iodinated contrast media conspicuity at a low kilovoltage can also improve visualization of systemic collateral supply from bronchial and nonbronchial arteries, a not-uncommon feature in some causes of PH (Fig 15). Although noise is increased at low kilovoltages, the associated increased contrast-to-noise ratio results in overall increased image quality (22).

Iodine-selective Imaging: Vascular Mapping

Similar to PBV imaging, which represents the iodine content of lung parenchyma, DECT can be used to generate maps of vascular iodine content, on which areas of vascular perfusion are color-coded according to their enhancement. These can be viewed in standard planar reformations or as a three-dimensional illustration of global intravascular enhancement.

Unlike at PBV imaging, this function can be used to identify intravascular pulmonary embolism and may help resolve the ambiguity of low Hounsfield unit values, which are caused by intravascular embolus, low contrast material enhancement, and partial volume effect with surrounding air in higher-order vessels. This function can improve visualization of vascular enhancement and has been evaluated for use in diagnosis of acute pulmonary embolism. These evaluations have demonstrated a high negative predictive value for exclusion of segmental pulmonary embolism (66).

Assessment of this imaging capability for the evaluation of PH is still in its infancy; however, the global overview of such imaging provides a

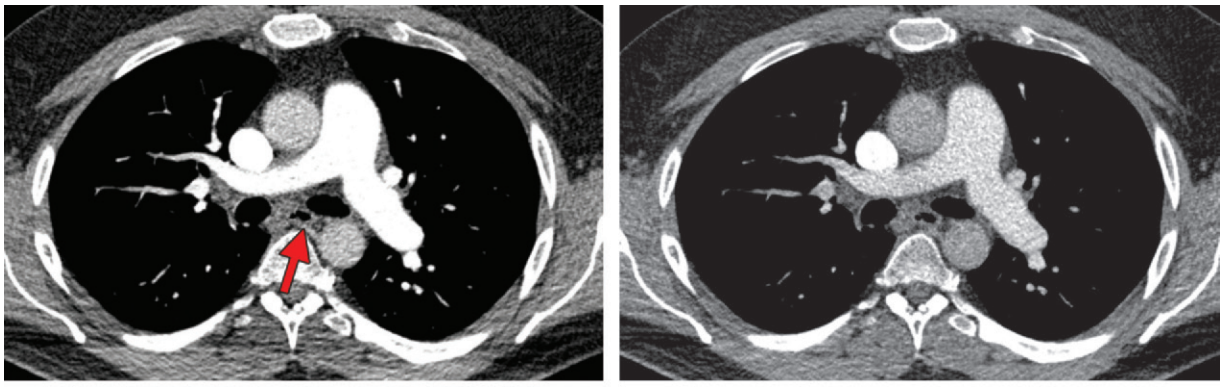

a. b.

Figure 15. Improved iodine conspicuity on low-kilovoltage images. Comparison of axial 100-kVp **(a)** and Sn 140-kVp **(b)** images in a 49-year-old man with CTEPH shows higher attenuation of the central and peripheral enhanced arteries and better visualization of a subtle enlarged bronchial artery (red arrow in **a**) on the 100-kVp image.

potential tool for evaluation of vascular morphology and underlying pathophysiology. It may also be used to help determine the cause of PH. For example, whereas a heterogeneous perfusion pattern would be expected in both CTEPH and idiopathic pulmonary arterial hypertension, stenosis and size variations in vessels are seen only in the former (Fig 16). Planning of surgical intervention in select cases or evaluation of disease progression may also be aided by these combined morphologic and functional displays.

Virtual Nonenhanced Imaging

Chronic thromboembolic disease can result in vascular calcification in a small number of patients. Such calcified thrombi are an important diagnostic feature but may be obscured by surrounding contrast material or difficult to differentiate from contrast material because of recanalization (50). This limitation can be overcome by using virtual nonenhanced (noncontrast) images, which can be readily generated by subtracting the iodine from the weighted-average images (9).

Visualization of Myocardial Ischemia

Right ventricular failure is the ultimate cause of death in most patients with PH. A direct correlation exists between right ventricular microvessel ischemia, as determined at myocardial scintigraphy, and right ventricular dysfunction in patients with PH (67). Ventricular perfusion maps generated at DECT can be used to assess left ventricular myocardial ischemia with 84% sensitivity and 94% specificity (68). Therefore, a similar principle could be applied for assessing right ventricular ischemia in patients with PH. However, this technique is still evolving and is hampered by the thinner myocardial thickness of the right ventricle, even in patients with substantial PH-induced right ventricular hypertrophy (Fig 17).

Quantitative Assessment of Pulmonary Blood Flow Dynamics

In addition to providing a perfusion map of pulmonary parenchymal iodine content, DECT enables simultaneous assessment of central vascular pulmonary arterial enhancement. A recent retrospective study of DECT found that when a standardized CTPA protocol was used, central pulmonary arterial enhancement in patients with PH was significantly higher than in patients without PH (64). Conversely, global volumetric PBV-determined parenchymal enhancement in patients with PH was reduced compared with in patients without PH. This DECT-measurable pattern of enhancement suggests a delay in pulmonary arterial to parenchymal transit as a consequence of increased PVR. Indeed, the ratio of central pulmonary arterial to parenchymal enhancement was significantly reduced in patients with PH, and this value correlated strongly with RHC-determined PVR. These findings mirror prior, more complex evaluations of pulmonary transit time at both contrast-enhanced (14) and time-resolved MR angiography (69,70). Such DECT parameters, and the effect of a second delayed time point of evaluation of parenchymal enhancement, are currently under prospective evaluation (Fig 18).

Limitations

The principle limitation of DECT in imaging of PH is the availability of CT systems capable of performing DECT. These higher-end systems have associated cost implications, although the development of competing dual-energy acquisition techniques from different vendors has partially redressed these costs. Because of the excessive noise on low-kilovoltage images, larger patients (generally > 105 kg) could not be imaged with first-generation dual-source imaging systems (71). In these same systems, the reduced DECT field

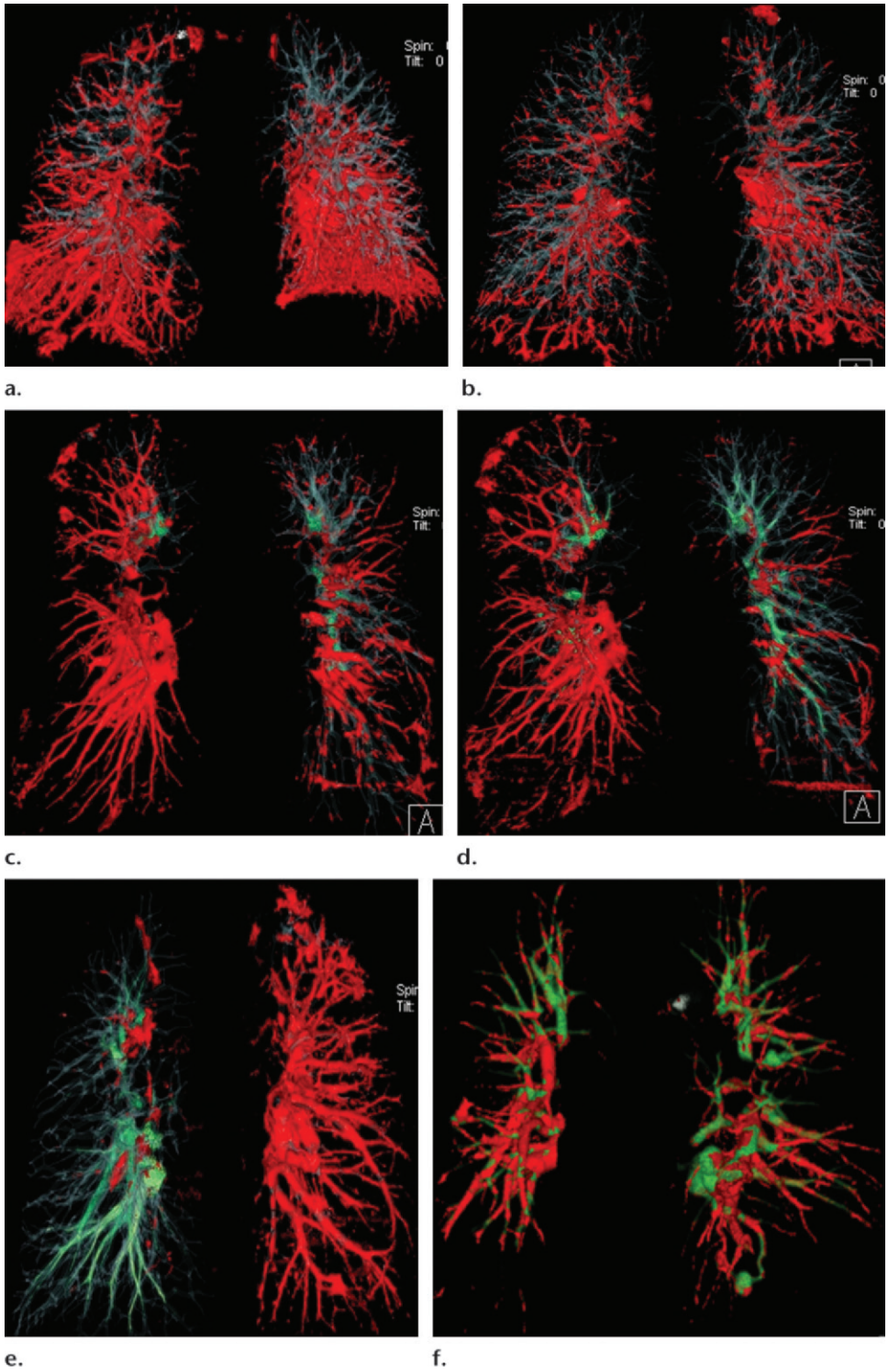

Figure 16. Pathologic variations in pulmonary vascular opacification on coronal iodine-selective DECT images in four patients. Blue and green = perfused vessels, red = reduced or absent perfusion. **(a, b)** In a 45-year-old man, acute bilateral lower lobe pulmonary emboli are seen in **a**, with posttreatment resolution seen in **b**. **(c, d)** In a 67-year-old woman who presented with shortness of breath, a large occlusive right main pulmonary artery embolus and small left upper lobe pulmonary emboli are seen in **c**. After thrombolysis and 7 months of anticoagulation therapy, persistent clot burden and evidence of chronic thromboembolic disease are seen in **d**. The patient was diagnosed with PH and was considered for thrombo-endarterectomy. **(e)** In a 59-year-old man with PH, tetralogy of Fallot, and chronic occlusion of the left lung pulmonary arteries, complete absence of perfusion is seen in the left lung. **(f)** In a patient with Osler-Weber-Rendu syndrome and PH, several left-sided perfused arteriovenous malformations are seen, as well as global reduced perfusion in the right lower lobe.

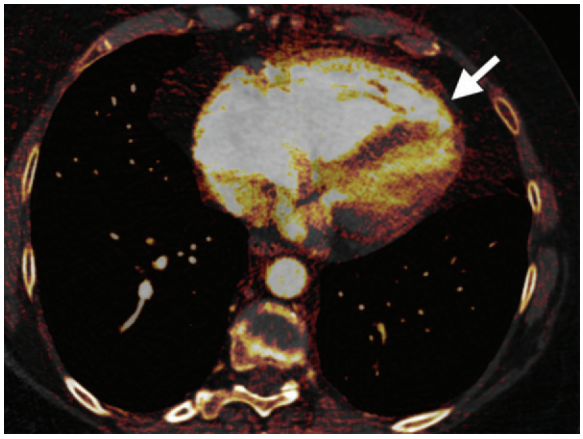

Figure 17. DECT depiction of myocardial ischemia in a 59-year-old woman with PH. Axial DECT-generated blood pool image shows dilated right cardiac chambers, with heterogeneous myocardial perfusion and a suspected focal perfusion defect in the right ventricular wall (arrow).

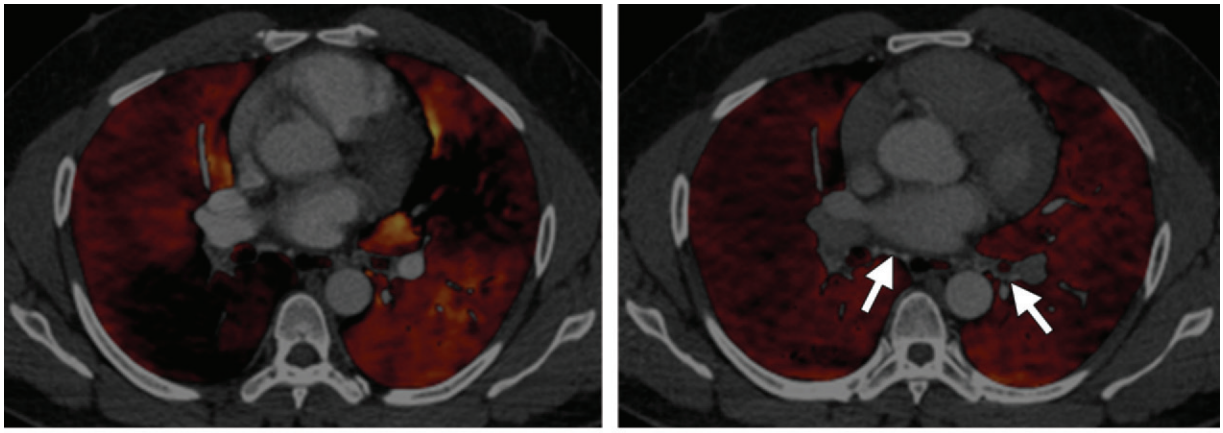

a. b.

Figure 18. Dual-phase acquisition of pulmonary enhancement images in a patient with CTEPH. **(a)** Axial initial whole-volume lung acquisition image at peak pulmonary arterial enhancement demonstrates large PBV defects bilaterally. **(b)** Axial delayed limited central volume acquisition image (obtained in the arterial phase 7 seconds after **a** to evaluate delayed parenchymal enhancement as part of a research protocol) shows equilibration of pulmonary parenchymal perfusion. This is likely due to the contribution of a physiologically significant bronchial arterial supply (arrows). Although such evaluation is still experimental, the findings may help explain the heterogeneity in patient responses to therapeutic intervention.

of view (26 cm) could also exclude the periphery of the lung in larger patients. These issues are effectively addressed in second-generation dual-source systems with selective tin photon shielding of the high-kilovoltage spectra, which permits 100-kVp and Sn 140-kVp combinations to image larger patients. The larger field of view of second-generation dual-source CT systems (33 cm) and rapid-kilovoltage systems (50 cm) has effectively removed patient thoracic diameter as a limiting consideration. Undoubtedly, the use of DECT necessitates the reconstruction and storage of thin-section datasets at low, high, and weighted-average kilovoltages, which may affect picture archiving and communication system (PACS) data storage.

A further practical limitation to the interpretation of DECT images is the variety of previously described common pseudodefects, which may require adaptation of the initial acquisition technique and familiarity with common pseudodefect patterns. In practice, these are rarely limiting, and their clinical impact can be mitigated by always interpreting PBV images in conjunction with weighted-average CTPA images. In general, DECT data reconstruction is rapid on a dedicated workstation. However, interpretation time may be lengthened by review of an increased number of images and requires additional training, experience, and expertise, although the additional information from PBV imaging may aid in interpretation of more complex cases.

Several other limitations should also be considered, especially as a trend toward quantitative DECT is emerging. The acquisition of reliable DECT PBV images requires use of consistent technique and timing to ensure that PBV perfusion surrogate qualitative or quantitative evaluations are reproducible. Further studies are required to confirm the value of proposed DECT features and metrics. These features should be

evaluated in conjunction with potentially confounding factors that may affect iodine density and distribution on PBV images, including cardiac disease, systemic and collateral supply to the lung parenchyma, and underlying lung parenchymal disease.

Although DECT holds promise for combining central vascular analysis with functional information regarding parenchymal enhancement, the validity of DECT PBV imaging compared with more established assessments of parenchymal perfusion (ie, V/Q scintigraphy and SPECT) is still under evaluation. Further studies of the consequences of DECT-derived metrics on patient treatment and outcome are required before a validated role for DECT in PH can be established.

Conclusion

DECT enables the simultaneous assessment of vascular anatomy, parenchymal morphology, functional perfusion, and cardiopulmonary status with no extra radiation dose. Lung perfusion assessed at PBV imaging correlates well with findings of nuclear medicine perfusion studies and in pulmonary embolism infers occlusive disease with increased risk of right heart dysfunction. PBV defects are accentuated in patients with PH, in particular but not limited to those with CTEPH. Perfusion inhomogeneities observed in PH closely reflect mosaic lung changes and may assist in severity assessment and prognostication. When combined with endovascular iodine-selective imaging, DECT may increase the detection of peripheral thromboembolic disease and provide additional information on the cause of mosaic changes. As with every novel technology, enthusiasm for applying DECT to the variety of indications and techniques for PH imaging must be tempered with awareness of its limitations and further investigations of how to surmount such limitations. Nevertheless, increasing evidence supports the use of DECT for imaging of PH and highlights its potential to evaluate PVR noninvasively. DECT may eventually replace scintigraphy and evolve into a superior anatomic and functional comprehensive "one-stop" test for PH diagnosis and severity assessment for surgical or drug therapy planning.

***Disclosures of Conflicts of Interest.*—J.L.B.:** *Activities related to the present article:* disclosed no relevant relationships. *Activities not related to the present article:* grants from Actelion Pharmaceuticals UK. *Other activities:* disclosed no relevant relationships. **I.V.:** *Activities related to the present article:* equipment, software support, and travel fees for educational lecture from Siemens Medical Systems. *Activities not related to the present article:* disclosed no relevant relationships. *Other activities:* disclosed no relevant relationships.

References

1. Galiè N, Hoeper MM, Humbert M, et al. Guidelines for the diagnosis and treatment of pulmonary hypertension: the Task Force for the Diagnosis and Treatment of Pulmonary Hypertension of the European Society of Cardiology (ESC) and the European Respiratory Society (ERS), endorsed by the International Society of Heart and Lung Transplantation (ISHLT). Eur Heart J 2009;30(20):2493–2537.
2. Simonneau G, Gatzoulis MA, Adatia I, et al. Updated clinical classification of pulmonary hypertension. J Am Coll Cardiol 2013;62(suppl 25):D34–D41.
3. Peña E, Dennie C, Veinot J, Muñiz SH. Pulmonary hypertension: how the radiologist can help. RadioGraphics 2012;32(1):9–32.
4. Bacon LJ, Peerbhoy SM, Wong E, et al. Current diagnostic investigation in pulmonary hypertension. Curr Respir Med Rev 2013;9(2):79–100.
5. Alvarez RE, Macovski A. Energy-selective reconstructions in x-ray computerized tomography. Phys Med Biol 1976;21(5):733–744.
6. Johnson TRC, Krauss B, Sedlmair M, et al. Material differentiation by dual energy CT: initial experience. Eur Radiol 2007;17(6):1510–1517.
7. Ko JP, Brandman S, Stember J, Naidich DP. Dual-energy computed tomography: concepts, performance, and thoracic applications. J Thorac Imaging 2012;27(1):7–22.
8. Kang MJ, Park CM, Lee CH, Goo JM, Lee HJ. Dual-energy CT: clinical applications in various pulmonary diseases. RadioGraphics 2010;30(3):685–698.
9. Lu GM, Zhao Y, Zhang LJ, Schoepf UJ. Dual-energy CT of the lung. AJR Am J Roentgenol 2012;199(suppl 5):S40–S53.
10. Bauer RW, Frellesen C, Renker M, et al. Dual energy CT pulmonary blood volume assessment in acute pulmonary embolism: correlation with D-dimer level, right heart strain and clinical outcome. Eur Radiol 2011;21(9):1914–1921.
11. Nef HM, Möllmann H, Hamm C, Grimminger F, Ghofrani HA. Pulmonary hypertension: updated classification and management of pulmonary hypertension. Heart 2010;96(7):552–559.
12. Janda S, Shahidi N, Gin K, Swiston J. Diagnostic accuracy of echocardiography for pulmonary hypertension: a systematic review and meta-analysis. Heart 2011;97(8):612–622.
13. Fukuchi K, Hayashida K, Nakanishi N, et al. Quantitative analysis of lung perfusion in patients with primary pulmonary hypertension. J Nucl Med 2002;43(6):757–761.
14. Skrok J, Shehata ML, Mathai S, et al. Pulmonary arterial hypertension: MR imaging-derived first-pass bolus kinetic parameters are biomarkers for pulmonary hemodynamics, cardiac function, and ventricular remodeling. Radiology 2012;263(3):678–687.
15. Grosse C, Grosse A. CT findings in diseases associated with pulmonary hypertension: a current review. RadioGraphics 2010;30(7):1753–1777.
16. Karçaaltıncaba M, Aktaş A. Dual-energy CT revisited with multidetector CT: review of principles and clinical applications. Diagn Interv Radiol 2011;17(3):181–194.

17. Kaza RK, Platt JF, Cohan RH, Caoili EM, Al-Hawary MM, Wasnik A. Dual-energy CT with single- and dual-source scanners: current applications in evaluating the genitourinary tract. RadioGraphics 2012;32(2):353–369.
18. Primak AN, Ramirez Giraldo JC, Liu X, Yu L, McCollough CH. Improved dual-energy material discrimination for dual-source CT by means of additional spectral filtration. Med Phys 2009;36(4):1359–1369.
19. Fornaro J, Leschka S, Hibbeln D, et al. Dual- and multi-energy CT: approach to functional imaging. Insights Imaging 2011;2(2):149–159.
20. Zou Y, Silver MD. Analysis of fast kV-switching in dual energy CT using a pre-reconstruction decomposition technique. In: Hsieh J, Samei E, eds. Proceedings of SPIE: medical imaging 2008—physics of medical imaging. Vol 6913. Bellingham, Wash: International Society for Optical Engineering, 2008; 691313.
21. Avrin DE, Macovski A, Zatz LE. Clinical application of Compton and photo-electric reconstruction in computed tomography: preliminary results. Invest Radiol 1978;13(3):217–222.
22. Godoy MCB, Heller SL, Naidich DP, et al. Dual-energy MDCT: comparison of pulmonary artery enhancement on dedicated CT pulmonary angiography, routine and low contrast volume studies. Eur J Radiol 2011;79(2):e11–e17. doi: 10.1016/j.ejrad.2009.12.030. Published February 11, 2010. Accessed January 5, 2013.
23. Schenzle JC, Sommer WH, Neumaier K, et al. Dual energy CT of the chest: how about the dose? Invest Radiol 2010;45(6):347–353.
24. Thieme SF, Johnson TRC, Reiser MF, Nikolaou K. Dual-energy lung perfusion computed tomography: a novel pulmonary functional imaging method. Semin Ultrasound CT MR 2010;31(4):301–308.
25. Marten K, Grabbe E. The challenge of the solitary pulmonary nodule: diagnostic assessment with multislice spiral CT. Clin Imaging 2003;27(3):156–161.
26. Coche E. Assessment of lung tumor response by perfusion CT. JBR-BTR 2013;96(3):172–174.
27. Sun H, Gao F, Li N, Liu C. An evaluation of the feasibility of assessment of volume perfusion for the whole lung by 128-slice spiral CT. Acta Radiol 2013;54(8):921–927.
28. Boroto K, Remy-Jardin M, Flohr T, et al. Thoracic applications of dual-source CT technology. Eur J Radiol 2008;68(3):375–384.
29. Remy-Jardin M, Faivre J-B, Pontana F, et al. Thoracic applications of dual energy. Radiol Clin North Am 2010;48(1):193–205.
30. Sokhi HK, Nair A, Ameli Renani SM, et al. Quantitative evaluation of dual-energy CT (DECT) perfused blood volume (PBV) measurements in a tiered contrast volume cohort [abstr]. In: Radiological Society of North America scientific assembly and annual meeting program. Oak Brook, Ill: Radiological Society of North America, 2011; 253.
31. Kim NH, Lang IM. Risk factors for chronic thromboembolic pulmonary hypertension. Eur Respir Rev 2012;21(123):27–31.
32. Remy-Jardin M, Pistolesi M, Goodman LR, et al. Management of suspected acute pulmonary embolism in the era of CT angiography: a statement from the Fleischner Society. Radiology 2007;245(2):315–329.
33. Sueyoshi E, Tsutsui S, Hayashida T, Ashizawa K, Sakamoto I, Uetani M. Quantification of lung perfusion blood volume (lung PBV) by dual-energy CT in patients with and without pulmonary embolism: preliminary results. Eur J Radiol 2011;80(3):e505–e509. doi:10.1016/j.ejrad.2010.10.011. Published November 10, 2010. Accessed January 5, 2013.
34. Fink C, Johnson TR, Michaely HJ, et al. Dual-energy CT angiography of the lung in patients with suspected pulmonary embolism: initial results. Rofo 2008;180(10):879–883.
35. Pontana F, Faivre J-B, Remy-Jardin M, et al. Lung perfusion with dual-energy multidetector-row CT (MDCT): feasibility for the evaluation of acute pulmonary embolism in 117 consecutive patients. Acad Radiol 2008;15(12):1494–1504.
36. Thieme SF, Johnson TRC, Lee C, et al. Dual-energy CT for the assessment of contrast material distribution in the pulmonary parenchyma. AJR Am J Roentgenol 2009;193(1):144–149.
37. Chae EJ, Seo JB, Jang YM, et al. Dual-energy CT for assessment of the severity of acute pulmonary embolism: pulmonary perfusion defect score compared with CT angiographic obstruction score and right ventricular/left ventricular diameter ratio. AJR Am J Roentgenol 2010;194(3):604–610.
38. Zhang LJ, Yang GF, Zhao YE, Zhou CS, Lu GM. Detection of pulmonary embolism using dual-energy computed tomography and correlation with cardiovascular measurements: a preliminary study. Acta Radiol 2009;50(8):892–901.
39. Thieme SF, Ashoori N, Bamberg F, et al. Severity assessment of pulmonary embolism using dual energy CT: correlation of a pulmonary perfusion defect score with clinical and morphological parameters of blood oxygenation and right ventricular failure. Eur Radiol 2012;22(2):269–278.
40. Apfaltrer P, Bachmann V, Meyer M, et al. Prognostic value of perfusion defect volume at dual energy CTA in patients with pulmonary embolism: correlation with CTA obstruction scores, CT parameters of right ventricular dysfunction and adverse clinical outcome. Eur J Radiol 2012;81(11):3592–3597.
41. Meinel FG, Graef A, Bamberg F, et al. Effectiveness of automated quantification of pulmonary perfused blood volume using dual-energy CTPA for the severity assessment of acute pulmonary embolism. Invest Radiol 2013;48(8):563–569.
42. Hoey ET, Agrawal SK, Ganesh V, Gopalan D, Screaton NJ. Dual energy CT pulmonary angiography: findings in a patient with chronic thromboembolic pulmonary hypertension. Thorax 2009;64(11):1012.
43. Nakazawa T, Watanabe Y, Hori Y, et al. Lung perfused blood volume images with dual-energy computed tomography for chronic thromboembolic pulmonary hypertension: correlation to scintigraphy with single-photon emission computed tomography. J Comput Assist Tomogr 2011;35(5):590–595.
44. Hoey ETD, Mirsadraee S, Pepke-Zaba J, Jenkins DP, Gopalan D, Screaton NJ. Dual-energy CT angiography for assessment of regional pulmonary perfusion in patients with chronic thromboembolic pulmonary hypertension: initial experience. AJR Am J Roentgenol 2011;196(3):524–532.
45. Renard B, Remy-Jardin M, Santangelo T, et al. Dual-energy CT angiography of chronic thromboembolic

disease: can it help recognize links between the severity of pulmonary arterial obstruction and perfusion defects? Eur J Radiol 2011;79(3):467–472.
46. Soler X, Kerr KM, Marsh JJ, et al. Pilot study comparing SPECT perfusion scintigraphy with CT pulmonary angiography in chronic thromboembolic pulmonary hypertension. Respirology 2012;17(1):180–184.
47. Lewczuk J, Piszko P, Jagas J, et al. Prognostic factors in medically treated patients with chronic pulmonary embolism. Chest 2001;119(3):818–823.
48. Fedullo P, Kerr KM, Kim NH, Auger WR. Chronic thromboembolic pulmonary hypertension. Am J Respir Crit Care Med 2011;183(12):1605–1613.
49. Lisbona R, Kreisman H, Novales-Diaz JDV, Derbekyan V. Perfusion lung scanning: differentiation of primary from thromboembolic pulmonary hypertension. AJR Am J Roentgenol 1985;144(1):27–30.
50. Castañer E, Gallardo X, Ballesteros E, et al. CT diagnosis of chronic pulmonary thromboembolism. RadioGraphics 2009;29(1):31–50; discussion 50–53.
51. Pitton MB, Kemmerich G, Herber S, Schweden F, Mayer E, Thelen M. Chronic thromboembolic pulmonary hypertension: diagnostic impact of multislice-CT and selective pulmonary-DSA [in German]. Rofo 2002;174(4):474–479.
52. Tunariu N, Gibbs SJR, Win Z, et al. Ventilation-perfusion scintigraphy is more sensitive than multidetector CTPA in detecting chronic thromboembolic pulmonary disease as a treatable cause of pulmonary hypertension. J Nucl Med 2007;48(5):680–684.
53. Bartalena T, Oboldi D, Guidalotti PL, et al. Lung perfusion in patients with pulmonary hypertension: comparison between MDCT pulmonary angiography with MinIP reconstructions and ^{99m}Tc-MAA perfusion scan. Invest Radiol 2008;43(6):368–373.
54. Thieme SF, Becker CR, Hacker M, Nikolaou K, Reiser MF, Johnson TRC. Dual energy CT for the assessment of lung perfusion: correlation to scintigraphy. Eur J Radiol 2008;68(3):369–374.
55. Thieme SF, Graute V, Nikolaou K, et al. Dual energy CT lung perfusion imaging: correlation with SPECT/CT. Eur J Radiol 2012;81(2):360–365.
56. Dartevelle P, Fadel E, Mussot S, et al. Chronic thromboembolic pulmonary hypertension. Eur Respir J 2004;23(4):637–648.
57. Kreitner KF, Kunz RP, Ley S, et al. Chronic thromboembolic pulmonary hypertension: assessment by magnetic resonance imaging. Eur Radiol 2007;17(1):11–21.
58. Thieme SF, Hoegl S, Nikolaou K, et al. Pulmonary ventilation and perfusion imaging with dual-energy CT. Eur Radiol 2010;20(12):2882–2889.
59. Rossi A, Attinà D, Borgonovi A, et al. Evaluation of mosaic pattern areas in HRCT with MinIP reconstructions in patients with pulmonary hypertension: could this evaluation replace lung perfusion scintigraphy? Eur J Radiol 2012;81(1):e1–e6. doi: 10.1016/j.ejrad.2010.09.032. Published November 4, 2010. Accessed January 7, 2013.
60. Pontana F, Remy-Jardin M, Duhamel A, Faivre JB, Wallaert B, Remy J. Lung perfusion with dual-energy multi-detector row CT: can it help recognize ground glass opacities of vascular origin? Acad Radiol 2010;17(5):587–594.
61. Heinrich M, Uder M, Tscholl D, Grgic A, Kramann B, Schäfers HJ. CT scan findings in chronic thromboembolic pulmonary hypertension: predictors of hemodynamic improvement after pulmonary thromboendarterectomy. Chest 2005;127(5):1606–1613.
62. Talwar A, Sarkar P, Patel N, Shah R, Babchyck B, Palestro CJ. Correlation of a scintigraphic pulmonary perfusion index with hemodynamic parameters in patients with pulmonary arterial hypertension. J Thorac Imaging 2010;25(4):320–325.
63. Fuld MK, Halaweish AF, Haynes SE, Divekar AA, Guo J, Hoffman EA. Pulmonary perfused blood volume with dual-energy CT as surrogate for pulmonary perfusion assessed with dynamic multidetector CT. Radiology 2013;267(3):747–756.
64. Ameli-Renani S, Ramsay L, Bacon J. Dual-energy computed tomography in the assessment of vascular and parenchymal enhancement in suspected pulmonary hypertension. J Thorac Imaging 2014;29(2):98–106.
65. Kang MJ, Park CM, Lee CH, Goo JM, Lee HJ. Focal iodine defects on color-coded iodine perfusion maps of dual-energy pulmonary CT angiography images: a potential diagnostic pitfall. AJR Am J Roentgenol 2010;195(5):W325–W330.
66. Krissak R, Henzler T, Reichert M, Krauss B, Schoenberg SO, Fink C. Enhanced visualization of lung vessels for diagnosis of pulmonary embolism using dual energy CT angiography. Invest Radiol 2010;45(6):341–346.
67. Gómez A, Bialostozky D, Zajarias A, et al. Right ventricular ischemia in patients with primary pulmonary hypertension. J Am Coll Cardiol 2001;38(4):1137–1142.
68. Ruzsics B, Lee H, Zwerner PL, Gebregziabher M, Costello P, Schoepf UJ. Dual-energy CT of the heart for diagnosing coronary artery stenosis and myocardial ischemia: initial experience. Eur Radiol 2008;18(11):2414–2424.
69. Jeong HJ, Vakil P, Sheehan JJ, et al. Time-resolved magnetic resonance angiography: evaluation of intrapulmonary circulation parameters in pulmonary arterial hypertension. J Magn Reson Imaging 2011;33(1):225–231.
70. Stevens GR, Fida N, Sanz J. Computed tomography and cardiac magnetic resonance imaging in pulmonary hypertension. Prog Cardiovasc Dis 2012;55(2):161–171.
71. Szucs-Farkas Z, Kurmann L, Strautz T, Patak MA, Vock P, Schindera ST. Patient exposure and image quality of low-dose pulmonary computed tomography angiography: comparison of 100- and 80-kVp protocols. Invest Radiol 2008;43(12):871–876.

Dual-Energy CT for Imaging of Pulmonary Hypertension: Challenges and Opportunities

Seyed Ameli-Renani, MBBS, FRCR • Farzana Rahman, MBBS, FRCR • Arjun Nair, MD, MRCP, FRCR • Laurie Ramsay, BMBCh • Jenny Louise Bacon, BM, MRCP • Alex Weller, MBBS, FRCR • Heminder K. Sokhi, MBBCh, FRCR • Anand Devaraj, MD, MRCP, FRCR • Brendan Madden, MBBS, FRCP, FRCPI • Ioannis Vlahos, MRCP, FRCR

RadioGraphics 2014; 34:1769–1790 • **Published online** 10.1148/rg.347130085 • **Content Codes:** CH CT

Page 1771
The advent of multidetector DECT offers the potential for qualitative and quantitative insights into pulmonary hemodynamics, particularly the distribution of central and peripheral vascular perfusion and the extent and variability of pulmonary parenchymal enhancement.

Page 1773
PBV imaging is in essence a "two–time-point" perfusion scan. The acquisition time forms the second time point, while the PBV calculation of the iodine content of the lung parenchyma, which can be separated and removed from the inherent physical density of the image, effectively acts as the precontrast initial time point.

Page 1773
Several studies have demonstrated that PBV imaging can be used to qualitatively assess areas of lung hypoperfusion, in a method similar to scintigraphy. As a result, PBV imaging is already well established for evaluating acute pulmonary embolism and has an emerging role in PH.

Page 1776
Furthermore, at PBV imaging analysis of CTEPH cases, the most severe pulmonary arterial features of CTEPH, including webs, bands, focal stenosis, and occlusion, are seen more frequently in segments with perfusion defects than in those with normal perfusion.

Page 1778
The combined intravascular and parenchymal enhancement information available at dual-energy CTPA with PBV imaging can also be used to determine whether areas of perfusion defect correspond to focal vascular obstruction, and consequently to determine the optimal therapeutic strategy.